U.PORTO

MESTRADO

MEDICINA E ONCOLOGIA MOLECULAR

Characterization of Prrxl1^{S119A} phospho-defective mouse:

Impact on the development of nociceptive neurons

Francisco Tomás Ribeiro

M
2020

DEPARTAMENTO DE BIOMEDICINA
UNIDADE DE BIOLOGIA EXPERIMENTAL
FACULDADE DE MEDICINA DA UNIVERSIDADE DO PORTO

Characterization of Prrxl1^{S119A} phospho-defective mouse: Impact on the development of nociceptive neurons

Francisco Tomás Ribeiro
Faculty of Medicine University of Porto
Instituto de Investigação e Inovação em Saúde (i3S)
Master´s in Molecular Medicine and Oncology

Supervisor: Carlos Manuel Gomes Reguenga, PhD
Co-supervisor: Ana Filipa Martins Dias, MSc

Aos meus pais, minhas maiores referências, pelo seu amor incondicional, pelo exemplo e por serem o porto seguro onde sinto que posso sempre voltar.

AGRADECIMENTOS

Agradeço ao Professor Doutor Carlos Reguenga e à Mestre Ana Filipa Dias terem aceitado ser meus orientadores. A sua amizade, disponibilidade, apoio e incentivo foram decisivos para realizar esta investigação. As discussões, as reflexões e as críticas construtivas que me proporcionaram revelaram-se fundamentais ao longo de todo o percurso. Gostaria também de agradecer por toda a paciência que tiveram comigo ao longo deste ano e meio.

Uma nota especial de agradecimento à Anabela Silvestre, pelo valioso apoio laboratorial que se revelou fundamental neste trabalho, bem como por toda a amizade, conversas e companhia.

Agradeço também ao Grupo *Pain Research*, da Faculdade de Medicina da Universidade do Porto / Instituto de Investigação e Inovação em Saúde, em particular ao Professor Doutor Filipe Monteiro, ao Rafael Miranda e à Marta Samina pelo apoio e pela forma amiga como me receberam, disponibilizando-se sempre para me ajudar.

Gostaria também de agradecer ao Grupo *Ageing & Stress*, em especial à Maria, à Filipa e à Catarina por sempre se mostrarem disponíveis para me ajudar. Estendo também este agradecimento a todo o restante pessoal do Departamento de Biologia Experimental da Faculdade de Medicina da Universidade do Porto que me ajudou e incentivou nos mais variados aspetos ao logo desta jornada, e que de uma forma ou de outra também acabou por participar neste trabalho. Um obrigado também à dona Lurdes.

Deixo também o meu agradecimento a todas as pessoas do biotério do i3S que possibilitaram este projeto, em especial à Doutora Sofia Lamas.

À Andreia o meu obrigada por todo o incentivo que se revelou fundamental sobretudo no final deste caminho.

Aos meus avós, Antero e Rosário, às minhas tias, Ana e Bela, e aos meus primos, Zé Pedro e João, agradeço o encorajamento e a colaboração em algumas fases do trabalho. E finalmente aos meus pais, Joaquim e Helena, que me ajudaram e apoiaram ao longo deste caminho, e sem os quais nada disto teria sido possível.

ABSTRACT

Prrxl1 is an important transcription factor (TF) involved in the development and maintenance of nociceptive neurons in dorsal spinal cord (dSC) and dorsal root ganglia (DRG). Accordingly, the ablation of this TF causes major abnormalities on embryos and post-natal mice. Moreover, Prrxl1 displays multiple phosphorylation profiles that evolves along SC and DRG development, acquiring specific patterns during neurogenesis and terminal differentiation phases. Phosphorylation at S119 site was shown to modulate Prrxl1 transcriptional activity in neuronal culture (Soares-dos-Reis et al., 2014). This study aimed to characterize a Prrxl1^{S119A} phospho-defective knock-in mouse in order to assess to what degree phosphorylation at S119 impacts on the development of the nociceptive system.

We successfully validated the Prrxl1^{S119A} mouse model as we verified that this mutation caused a phosphorylation pattern similar to the one previously observed in neuronal cell line (Soares-dos-Reis et al., 2014). We then quantified the expression of selected Prrxl1 target genes by qPCR and assessed possible defects in dSC/DRG through morphological analysis in embryonic stages. Furthermore, we performed functional studies to evaluate post-natal mice response to noxious stimuli resorting to formalin-induced inflammatory pain test.

We were not able to discern major if any alterations in our knock-in mouse model such as phenotypical defects in the pain pathway, changes in gene expression related to the phospho-defective mutation or spinal cord morphology variations. Most of our results turned to be inconclusive due mainly to sample variability.

As a whole, our findings went a step forward in the understanding of the significance of the phosphorylation at Prrxl1^{S119A} site in the development of nociceptive neurons, but nonetheless additional research is required. Capitalizing on our experience, this work also provides indications and future directions to further assess and characterize Prrxl1^{S119A} mouse model focusing on the age- and tissue-specific behaviour of pS119.

Keywords: development; nociception; phosphorylation; Prrxl1; spinal cord

RESUMO

Prrxl1 é um importante fator de transcrição envolvido no desenvolvimento e manutenção dos neurónios nociceptivos da medula espinal dorsal e dos gânglios da raiz dorsal. A ausência deste fator de transcrição causa anomalias significativas tanto em estádios embrionários como pós-natais. Além disso, este fator de transcrição apresenta múltiplos padrões de fosforilação que evoluem ao longo do desenvolvimento da medula espinal e dos gânglios da raiz dorsal, adquirindo padrões específicos durante a neurogénese e em fazes terminais da diferenciação. Foi demonstrado que a fosforilação no local S119 permite a modulação da atividade transcricional em culturas neuronais (Soares-dos-Reis et al., 2014). O presente estudo tem como objetivo a caracterização de ratinhos *knock-in* Prrxl1^{S119A}, de modo a melhor compreender de que forma a fosforilação do local S119 impacta o desenvolvimento do sistema nociceptivo

Foi validado com sucesso o modelo de ratinho Prrxl1^{S119A} visto que verificámos que a fosfo-mutação causa um padrão de fosforilação semelhante àquele observado em linhas celulares neuronais (Soares-dos-Reis et al., 2014). De seguida, quantificámos por qPCR a expressão de alguns genes-alvo do fator de transcrição Prrxl1 e avaliámos possíveis anomalias na medula espinal e gânglios através de análise morfológica em estádios embrionários. Para além disto, estudos funcionais através da injeção de formalina em ratinhos pós-natais permitiram-nos avaliar a resposta a estímulos nociceptivos

Não foi possível identificar alterações significativas no nosso modelo *knock-in* como, por exemplo, defeitos fenotípicos na via da dor, alterações na expressão génica relacionadas com a presença da fosfo-mutação Prrxl1^{S119A}, ou variações na morfologia da medula espinal. A maior parte dos nossos resultados acabou por ser inconclusiva devido à grande variabilidade entre amostras.

No seu conjunto, as nossas descobertas deram um importante passo em frente no que à fosforilação do local Prrxl1^{S119A} diz respeito, sendo que mais estudos necessitarão de ser feitos. Este trabalho também proporciona indicações e direções futuras para melhor caracterizar este modelo de ratinho Prrxl1^{S119A}, com especial incidência na fosforilação dependente da idade e do tecido do local S119.

***Palavras-chave**:* desenvolvimento; nocicepção; fosforilação; Prrxl1; medula espinhal.

TABLE OF CONTENTS

LIST OF FIGURES

LIST OF TABLES

LIST OF ABREVIATIONS

ABC	Avidin-biotin complex
bHLH	Basic helix-loop-helix
Bp	Base pair
Brn3a	Brain-specific homeobox/POU domain protein 3A
BSA	Bovine serum albumin
Ccdc68	Coiled-coil domain containing 68
Cck	Cholecystokinin
CDNA	Complementary deoxyribonucleic acid
CFOS	FOS proto-oncogene
ChodI	Cholesterol oxidase
CNS	Central nervous system
Co-IP	Protein complex immunoprecipitation
CRISPR	Clustered regularly interspaced short palindromic repeats
DAB	3,3'-Diaminobenzidine
dI	Dorsal interneurons
dIL	Late-born dorsal interneurons
DNA	Deoxyribonucleic acid
DREZ	Dorsal root entry zone
DRG	Dorsal root ganglia
dSC	Dorsal spinal cord
DTT	Dithiothreitol
GABA	γ-aminobutyric acid
Galr1	Galanin receptor 1
Gbx1	Gastrulation brain homeobox 1
GLB	Gel loading buffer
HCl	Hydrochloric acid
HRP	Horseradish peroxidase
i3S	Instituto de Investigação e Inovação em Saúde
IHC	Immunohistochemistry
KO	Knock-out
L	Litre
Lbx1	Ladybird homeobox 1
Lhx1	LIM homeobox 1
Lhx5	LIM homeobox 5
Lmo3	LIM domain only 3

Lmx1b	LIM homeobox transcription factor 1 beta
mg	Milligram
mL	Millilitre
NaOH	Sodium hydroxide
ND7/23	Mouse neuroblastoma x rat neuron hybrid
nm	Nanometre
OCT	Optimal cutting temperature
Pax2	Paired box 2
PBS	Phosphate-buffered saline
PCR	Polymerase chain reaction
PFA	Paraformaldehyde
PIN1	Peptidyl-prolyl cis-trans isomerase NIMA-interacting 1
PNS	Peripheral nervous system
Prrxl1	Paired related homeobox protein-like 1
qPCR	Quantitative polymerase chain reaction
RFLP	Restriction fragments length polymorphism
RNA	Ribonucleic acid
SC	Spinal cord
SDS-PAGE	Sodium dodecyl sulphate–polyacrylamide gel electrophoresis
TBS	Tris-buffered saline
TF	Transcription factor
Tlx3	T cell leukaemia homeobox 3
Tris	Tris(hydroxymethyl)aminomethane
TrkA	Tyrosine kinase receptor A
TrkC	Tyrosine kinase receptor C
WB	Western blot
Whrn	Whirlin
Wt	Wild-type
µg	Microgram
µL	Microlitre

CHAPTER 1

INTRODUCTION

1.1 The nervous system

The nervous system is responsible for “monitoring and responding to changes in the internal and external environment”, as well as for perception, behaviour, and memory (Farley, Johnstone, Hendry, & McLafferty, 2014). This system is thus in charge of coordinating all activities of the body. The nervous system integrates both a central part (central nervous system), including the brain and spinal cord, and a peripheral part (peripheral nervous system), encompassing all nervous tissue outside the CNS, connecting it to other areas of the body. These two systems interact with each other and with the rest of the body, allowing for self- and environmental awareness. For this to be possible, sensation and sensory processes are required.

Sensation, as described by Purves et al. (2004) “entails the ability to transduce, encode, and ultimately perceive information generated by stimuli”. These stimuli can, as previously mentioned, be generated in response to both the internal and external environments, thus helping us navigate the world around us. Examples of sensory modalities are hearing, vision or pain. These stimuli (light or sound, for example) must be converted and encoded to be perceived by the brain and, if required, trigger a response.

1.2 Pain and nociception

Of all the different sensory modalities, pain is the one by which the body tries to avoid damage (or further damage) to itself. Pain, as defined by the *International Association for the Study of Pain*, is “an unpleasant sensory and emotional experience associated with, or resembling that associated with, actual or potential tissue damage” (Loeser & Treede, 2008; Merskey, Mumford, Nathan, Noordenbos, & Sunderland, 1994; Raja et al., 2020; Treede, 2018).

Nociception, on the other hand, can be discerned from pain: while the latter refers to a somewhat subjective experience - being only present in the individual that feels it, nociception encompasses “the neural processes of encoding and processing noxious stimuli” (Loeser & Treede, 2008). In fact, one can occur without the other (Loeser & Treede, 2008; Treede, 2018). In short, pain “perception is a product of the brain’s abstraction and elaboration of sensory input” (Basbaum & Jessell, 2000).

Even though pain evolved as somewhat of a warning system for the body, some problems can cause it to be very damaging to its normal functioning. This is the case of neuropathic pain: while nociceptive pain serves a purpose to avoid any or further damage (being usually caused by actual or possible harm to the body’s tissues), neuropathic pain is caused by

damage to the somatosensory nervous system itself, and it leads to the malfunction of the nociceptive system, causing it to respond in an abnormal manner to stimuli. Symptoms of such pain can be heightened pain response to a noxious stimulus (hyperalgesia), or pain response elicited by apparently innocuous stimuli (allodynia) (Crofford, 2015; Jensen & Finnerup, 2014; Merskey et al., 1994). These chronic conditions no longer possess any advantage in terms of alerting the individual towards possible damage to the body, which makes this type of pain non-beneficial (Basbaum & Jessell, 2000). Pathologies involving chronic pain are fairly common throughout the world (Breivik, Collett, Ventafridda, Cohen, & Gallacher, 2006; Nahin, 2015), therefore research is needed to provide further insight in this field.

1.3 The pain pathway

For the noxious stimuli to be felt by the individual and for an accurate response to be triggered, a signal must be conveyed from the "site of detection" to the thalamus and specific areas of the cerebral cortex, where it is processed (*ascending pathway*) (Basbaum & Jessell, 2000). An accurate response can then be generated and transmitted to target muscles (via the *descending pathway*) (Yam et al., 2018).

Nociceptors are relatively unspecialized nerve cell endings, which detect noxious stimuli, transducing these into an action potential (Purves et al., 2004). As seen in Figure 1, these nociceptive afferent fibres enter the spinal cord and terminate in the dorsal horn of the spinal cord, where they synapse with second order neurons.

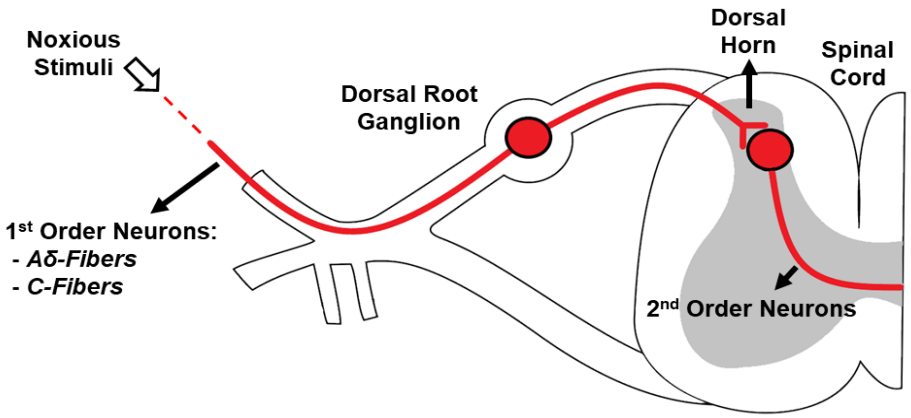

***Figure 1* - Transversal cut of a dorsal root ganglion and spinal cord.** Nociceptor terminals of afferent fibres (first order neurons), with their soma located within dorsal root ganglia, sense the noxious stimuli, and convey the signal to second order neurons located in the dorsal horn of the spinal cord (represented). In turn, second order neurons transduce and lead the signal upward, toward the brain.

Various classes of somatosensory afferents exist, but nociceptive stimuli input is conveyed through Aδ- and C-fibres (Figure 2A). These two distinct types of fibres carry impulses at different speeds. C-fibres possess no myelin sheath, which is not the case for Aδ-fibres. The latter conduct impulses at higher speeds. The difference in conducting properties between these two types of nociceptive neurons explains why two waves of pain can be felt (Figure 2B) (Julius & Basbaum, 2001). Afferent fibres also project differently, targeting distinct laminae in the spinal cord: while touch and proprioception sensations target II$_{inner}$-V and more ventral laminae, respectively, nociceptors target laminae I and II (Figure 2A) (Lai et al., 2016). In turn, neurons located at the laminae targeted by nociceptive afferents (second order neurons) receive the signal and convey it to specific areas in the brain where this sensory information can be interpreted, thus contributing to the experience of pain (Yam et al., 2018). On the flip side, a response to noxious stimuli can be conveyed through motor neurons (efferent fibres), via the spinal cord, and targeting reflex muscles, which in turn effectively react to the noxious stimuli, thus avoiding any or further injury (Yam et al., 2018).

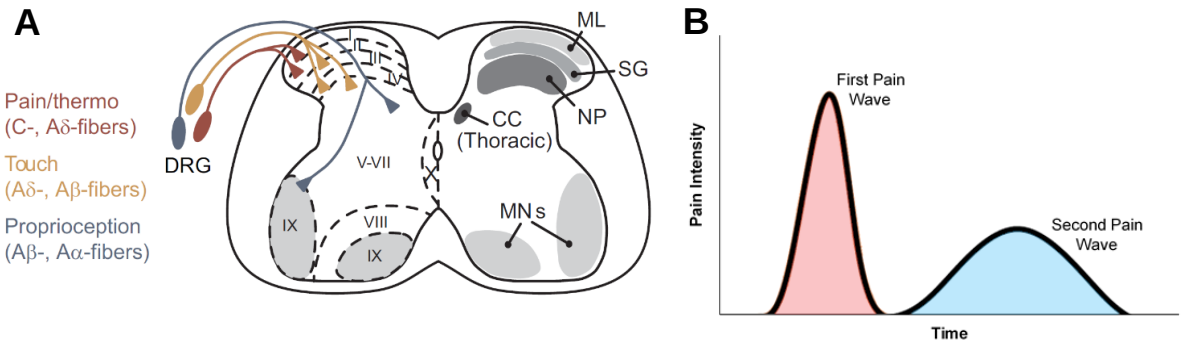

***Figure 2* - Lamination of the spinal cord and pain waves**. **A**: The various classes of afferent fibres and the laminae they target. First order neurons responsible for sensing noxious stimuli (along with thermosensitive neurons) project to laminae I-II (fibres C- and Aδ-) (Adapted from Lai et al. (2016)); **B**: "Pain waves" generated due to the difference between diameter of the fibres conducting the impulse. Aδ-fibres (in blue) possess a myelin sheet, which conduct signals at higher speeds when compared to C-fibres (unmyelinated, in green). This difference in properties allow for the possibility of two "pain waves".

The spinal cord is composed of white matter, consisting of myelinated axons, and grey matter, mainly composed of neuronal soma. The latter, located in the central part of the spinal cord, has a characteristic butterfly shape, and is divided into ten somewhat parallel laminae, called *laminae of Rexed (Rexed, 1954; Todd, 2010)*. These laminae have correspondent anatomical names: marginal layer (lamina I), *substantia gelatinosa* (lamina II), *nucleus proprius* (laminae III-V) and motor neurons (lamina IX) (Lai et al., 2016). Moreover, while laminae VIII and IX correspond to the ventral horn of the spinal cord, laminae I-VI relate to the dorsal horn. As mentioned previously, the top two laminae of the

dorsal horn (laminae I and II) are targeted by nociceptive primary afferents (Figure 2A). Once fully developed, the spinal cord's grey matter becomes organized in a laminated structure, as illustrated in Figure 2A. Broadly speaking, neurons in the dorsal part of the spinal cord tend to be directed to processing and relaying sensory information, while those in the ventral part gives rise to motor and interneurons involved in motor processes (Muller et al., 2002). As such, the spinal cord appears as the main relay centre for pain processing, as it receives the impulses from nociceptors in the periphery and transmits them up the pathway toward the brain, where a proper response is eventually generated.

1.4 Development and patterning of the spinal cord

At the dorsal horn, the laminated structure development occurs under strict control of proneural genes, responsible for encoding bHLH (*basic Helix-loop-Helix*) transcription factors. These TFs trigger cell differentiation, which causes the specification of progenitor cell identity. Two main neurogenesis waves occur, leading to the formation of different populations. The first wave, occurring between embryonic day 10.5 and 11.5, leads to the formation of 6 distinct subpopulations within the dorsal neural tube: dI1, dI2, dI3, dI4, dI5 and dI6 (Cheng et al., 2004). Distinction between subpopulations can be made according to the combination of homeodomain transcription factors expressed by each one (Figure 3) (Caspary & Anderson, 2003). Such subpopulations can however be split into two major neuronal classes: *class A*, that is Lbx1-independent (dI1-dI3); and *class B*, Lbx1-dependent neurons (dI4-dI6) (Figure 3) (Cheng et al., 2005; Muller et al., 2002). The second neurogenesis wave occurs at a later moment, between embryonic day 12 and 14.5, and gives rise to two new late-born subpopulations: dIL_A and dIL_B (Cheng et al., 2004; Helms & Johnson, 2003).

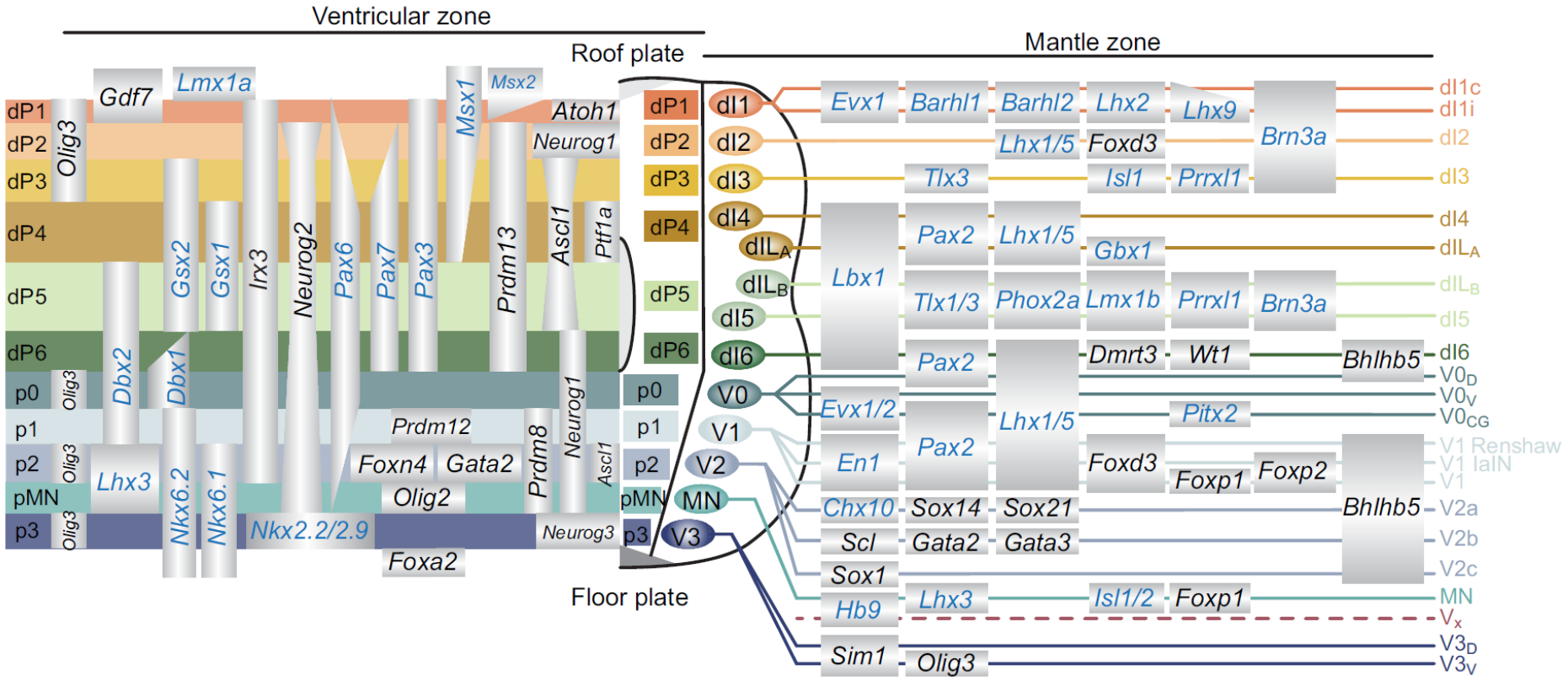

***Figure 3* - Representation of transcription factor diversity** involved in the patterning of the developing spinal cord before migration throughout takes place. The combinatorial expression of these transcription factors leads to the development of particular cell types, organizing the spinal cord into its laminated shape (Adapted from Lai et al. (2016).

After the various populations have arisen from their progenitor domains, by the later stages of development, neuronal migration occurs (Lai et al., 2016). This migration organizes the neurons throughout the spinal cord, from the dorsal aspect to its most dorsal regions. Thus, while progenitor domains establish what population a certain neuron integrates, and their possible subsets, they do not directly determine the region they will settle and reside in the adult spinal cord (Figure 4).

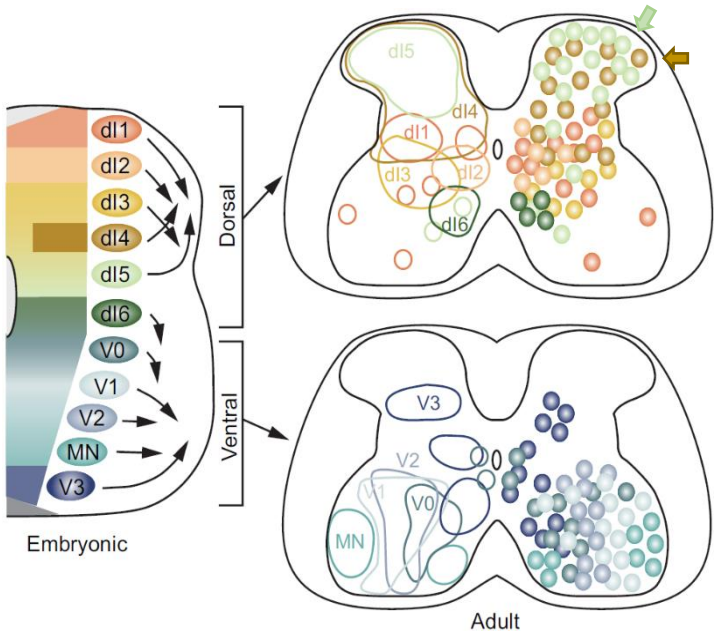

***Figure 4* - Neuronal migration during the development of the spinal cord**. After being derived from their progenitor domains, the various populations of neurons migrate and distribute themselves throughout the spinal cord, not remaining for the most part in their correspondent birthplaces (adapted from Lai et al. (2016).

1.5 Glutamatergic versus GABAergic

Class B neurons (Lbx1-dependent) present in the dorsal spinal cord can be divided into two major groups, depending on their main neurotransmitter (Cheng et al., 2004). One of the groups possesses excitatory properties, whilst the other presents inhibitory characteristics.

While excitatory neurons, also called glutamatergic neurons, use glutamate as their main neurotransmitter, and originate from the late-born subpopulation dIL_B, inhibitory neurons, or GABAergic neurons, use γ-aminobutyric acid (or GABA) and/or glycine, and arise from late-born subpopulation dIL_A.

As previously mentioned, these two late-born populations are specified during the second wave of neurogenesis, and they share the same progenitor domain: they both derive from

dI4 and dI5 cells (Caspary & Anderson, 2003), which end up settling in the dorsal-most aspect of the adult spinal cord (Figure 4, dark-brown and light-green arrows, respectively) (Lai et al., 2016). Since they originate from populations of neurons belonging to class B, they both express Lbx1 (Muller et al., 2002). Lbx1 is also known to assure an inhibitory GABAergic fate (Cheng et al., 2005), which occurs in dIL_A, by inducing certain inhibitory transcription factors, including Lbx1, Pax2, Lhx1, Lhx5 and Gbx1, and repressing excitatory TFs, like Tlx3, Lmx1b, Brn3a and Prrxl1 (Figure 4) (Lai et al., 2016).

Paradoxically, Lbx1 is also expressed in dIL_B excitatory glutamatergic neurons. Tlx3, however, acts as an antagonist to Lbx1: its expression counteracts the effect of Lbx1 on determining a GABAergic fate, to promote glutamatergic differentiation (Cheng et al., 2005). Besides Tlx3, other homeodomain transcription factors were shown to be required for the differentiation and maintenance of glutamatergic dorsal spinal cord neurons. One of those is *Paired-related homeobox protein-like 1* (Prrxl1), previously known as *Dorsal Root Ganglia 11* (DRG11).

1.6 Paired related homeobox protein-like 1

Prrxl1 is a paired-like homeodomain transcription factor, expressed in the developing dorsal horn of the spinal cord and in DRG sensory neurons (Chen et al., 2001). Its expression levels in adult life are low, however, during inflammatory pain, an increase in their expression was observed, pointing toward a role in sensitization of nociceptive neurons (C. Monteiro, Rebelo, Galhardo, Reguenga, & Lima, 2011).

Previous studies involving Prrxl1-null mice identified several defects when compared to wild-type counterparts. Phenotypically, Prrxl1$^{-/-}$ mice were smaller and presented characteristic skin lesions just above the tail, as seen in Figure 5A. They also displayed reduced sensitivity to noxious stimuli (Figure 5B) and severely diminished lifespan (Chen et al., 2001; Rebelo, Chen, Anderson, & Lima, 2006).

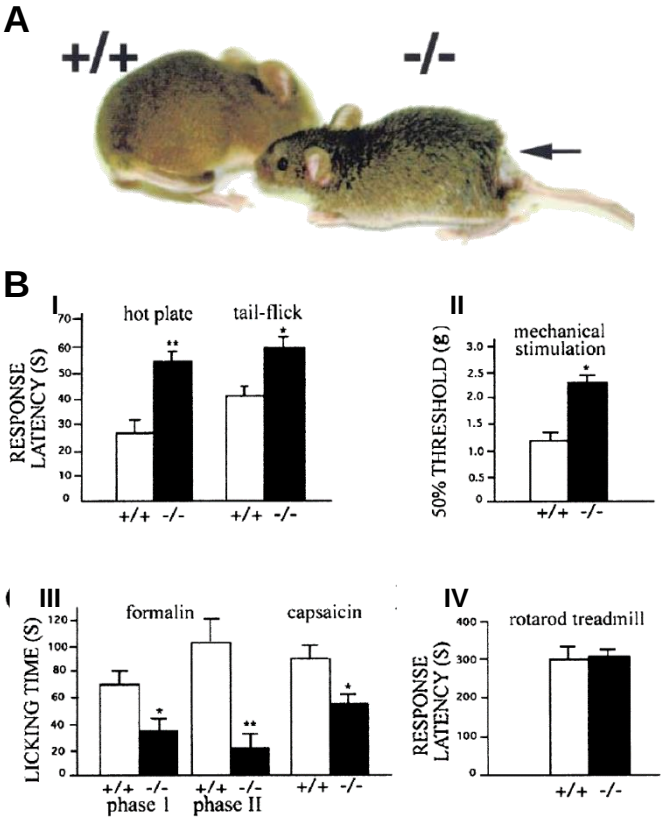

***Figure 5* - Prrxl1 knock-out comparison and functional tests**. **A**: Prrxl1-null mouse (on the right) next to wild-type counterpart of the same litter (on the left). Phenotypically, the Prrxl1$^{-/-}$ mice were smaller and weight less. A characteristic skin lesion was also observed (arrow) (Adapted from Chen et al. (2001). **B**: Prrxl1-null mice also displayed reduced sensitivity to nociceptive and mechanical stimuli. Various tests were performed: thermal sensitivity, von-Frey, chemical nociception, and sensorimotor function tests. **I** – both the hot plate and tail flick tests yielded results where the Prrxl1$^{-/-}$ mice responded in a delayed manner; **II** – mechanical stimulation test indicated that the necessary threshold to produce a response in the Prrxl1-null mice was significantly higher; **III** – response to chemical stimuli was also attenuated in the Prrxl1$^{-/-}$, as they responded with significantly reduced paw licking; Tests **I-III** yielded convergent results, pointing toward reduced sensitivity in the Prrxl1-null mice. Its sensorimotor functions (**IV**) were however unaffected, possibly due to the involvement of a different type of fibre necessary for this type of function.

Additionally, Prrxl1$^{-/-}$ animals displayed defects in afferent fibre projections in the dorsal horn during the intermediate stages of development (Figure 6). These afferent fibres are intended to enter the dorsal horn of the spinal cord at around E12.5, where synapses with second order neurons will eventually occur. However, since by E14.5 fibres had already invaded the dorsal horn of Prrxl1$^{-/-}$ mice, these defects were considered to result from a delay rather than a complete block of the ingrowth of afferent fibres (Figure 6D).

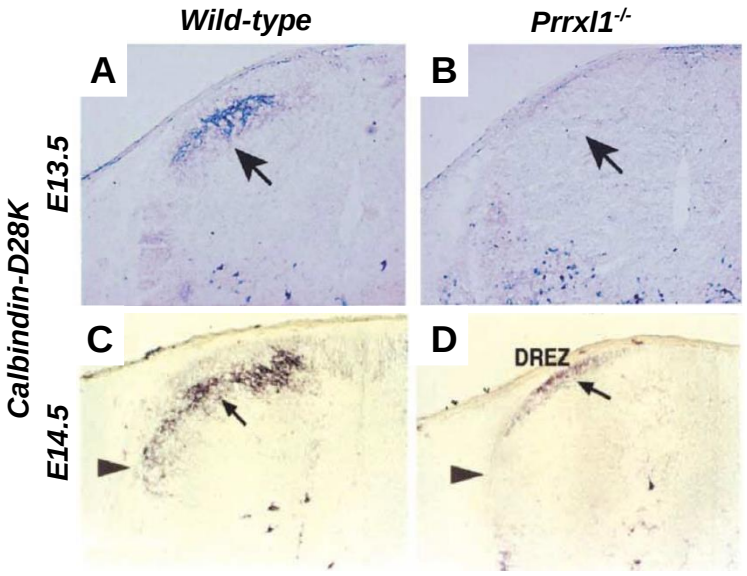

***Figure 6* - Late afferent fibre projection in Prrxl1-null mice**. **A** and **B**: By E13.5, afferent fibres in the wild-types have already penetrated the dorsal horn of the spinal cord (on the left), while in Prrxl1-null mice afferent fibres are yet to enter the Dorsal Root Entry Zone (DREZ) (on the right). **C** and **D**: At E14.5, significant ingrowth of afferent fibres is registered in wild-type individuals (on the left), while in Prrxl1-null mice the afferents only appear to have began to penetrate the dorsal horn. These results are indicative of a delay, rather than a block of afferent fibre projection into the dorsal horn of the spinal cord (adapted from Chen et al. (2001).

Morphological abnormalities in the superficial dorsal horn of the spinal cord were also reported, due to the ablation of most of the glutamatergic neurons in that region. This ablation occurs due to the loss of most, but not all, Prrxl1-expressing glutamatergic neurons. The remaining glutamatergic neurons still express Tlx3 and Lmx1b, and are considered Prrxl1-independent neurons (Figure 7E). This signifies that populations of Prrxl1-independent neurons (such as the previously mentioned Prrxl1^{-}/Tlx3^{+}/Lmx1b^{+} glutamatergic subsets and GABAergic neurons) are preserved in equivalent numbers to those in wild-type individuals. These results indicate that Prrxl1-dependent neurons do not persist, and instead degenerate. The total number or neurons is therefore reduced, which impacts on the dorsal horn morphology (Figure 7A-D, dashed line), leading to the ablation of the most superficial part of the dorsal horn of the spinal cord of Prrxl1-null mice. The ablation of such neurons in the KO mice indicates that Prrxl1, aside from being required for the correct wiring of primary afferent nociceptive neurons (Chen et al., 2001), also appears to play a role in maintaining a subset of glutamatergic neurons after its specification (Rebelo et al., 2006).

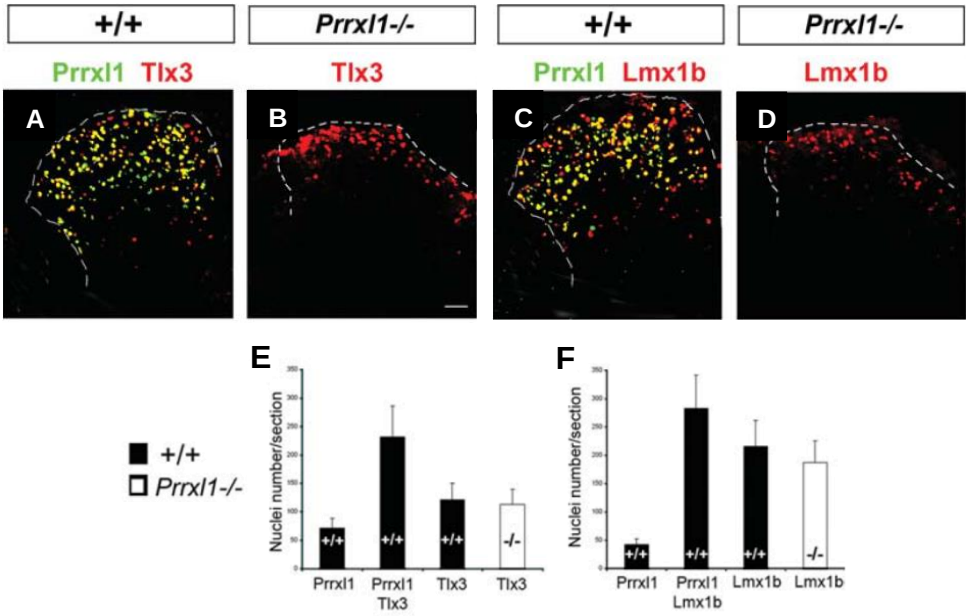

***Figure 7* - Dorsal horn glutamatergic neurons in Prrxl1-null mice**. The number of glutamatergic neurons is affected in Prrxl1-null mice. However, this reduction of glutamatergic neurons appears to only affect the ones that are Prrxl1-dependent. A significant loss of dorsal horn region can be observed (dashed line) (adapted from Rebelo et al. (2010)).

Further studies into the implications of the loss of the uppermost parts of the dorsal horn region uncovered a reduction in cFos expression in Prrxl1$^{-/-}$ mice after noxious stimulation (Figure 8*)*. cFos expression increased upon nociceptive stimulation and is thus commonly used as a marker of synaptic transmission between the DRG and the spinal cord. The

observed cFos reduction in Prrxl1$^{-/-}$ mice, however, was not seen in the deeper portions of the dorsal horn, which is likely due to undisturbed peripheral nociceptive innervation in these regions of the spinal cord (Figures 8B and 8F) (Rebelo et al., 2010). While the loss of Prrxl1 impacts on the survival of some DRG neurons (small diameter primary afferent neurons), a significant portion of DRG neurons persist (Rebelo et al., 2006). It is thus very likely that these are neurons that synapse with cFos^{+} neurons in the deeper dorsal horn (Rebelo et al., 2010). This finding further indicates that the previously observed post-natal death of DRG neurons (Rebelo et al., 2006) is possibly related to lack of connection with their targets in the superficial dorsal horn. The loss of this region of the dorsal horn is clearly seen in the camera lucida drawings on the right of Figure 8 (Figure 8C and 8G).

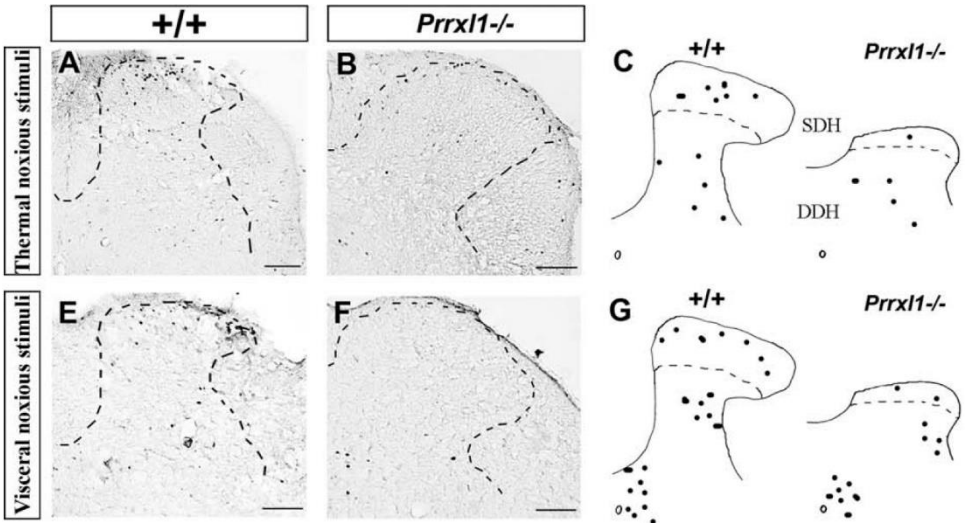

***Figure 8* - Observable reduction in cFos^{+} neurons after two different types of noxious stimulation**. The number of cFos-expressing neurons is quite reduced when comparing wild-type to Prrxl1$^{-/-}$ mice. However, deeper dorsal horn neurons are still cFos^{+} (adapted fromRebelo, Reguenga, Lopes, and Lima (2010)).

Prrxl1 transcriptional control has been demonstrated to occur in a variety of ways. This homeodomain transcription factor can control its own expression levels via a mechanism of self-repression (C. B. Monteiro et al., 2014). The direct and indirect action of the transcription factor Tlx3 also allows for a strict regulation of its activity, either by transcriptional regulation or through the induction of protein phosphorylation (Regadas et al., 2014). Prrxl1 phosphorylation can be observed through band patterns upon SDS-PAGE analysis. This phosphorylation profile has been shown to vary along development. A total of four bands have been identified throughout the various stages of development, as seen in Figure 9 (Soares-dos-Reis et al., 2014). Bands were named 1 to 4, from the slowest migrating band (higher number of phosphorylations) to the fastest (lower number of

phosphorylations). Prrxl1 phosphorylation is not only age-dependent, as it has been shown to vary throughout development, but also tissue-specific, since western-blot analysis from the dorsal spinal cord and dorsal root ganglia display distinct band patterns, even when considering the same developmental timepoints (Soares-dos-Reis et al., 2014). While In early developmental ages (from E10.5 to E14.5) band patterns in dSC and DRG coincide, both displaying the first upper bands (bands 1 and 2), after E16.5 band 1 is progressively lost, being differentially replaced: in dSC it is replaced by band 4, while in DRG band 3 seems to take its place. This substitution by the lower bands appears to indicate gradual protein dephosphorylation as development progresses. Band 2 however was maintained throughout the different ages. Prrxl1 overexpressed in ND7/23 cell (DRG-derived cell line), used in previous *in vitro* studies, presents a band pattern similar to the one observed in P0 dSC (Figure 9) (Soares-dos-Reis et al., 2014). Post-translational modifications such as phosphorylation are important since they can alter proteins function through conformational variations in its structure. Therefore, these modifications act as molecular switches, regulating the affinity and selectivity towards certain protein-DNA interactions, which leads to a shift in protein function (Cohen, 2000; Hunter, 2012). Co-IP studies on Prrxl1 also indicated toward the involvement of the protein isomerase PIN1 in a mechanism of phosphorylation-mediated conformational changes that regulates Prrxl1 activity in the development of the nociceptive system (Soares-Dos-Reis et al., 2017).

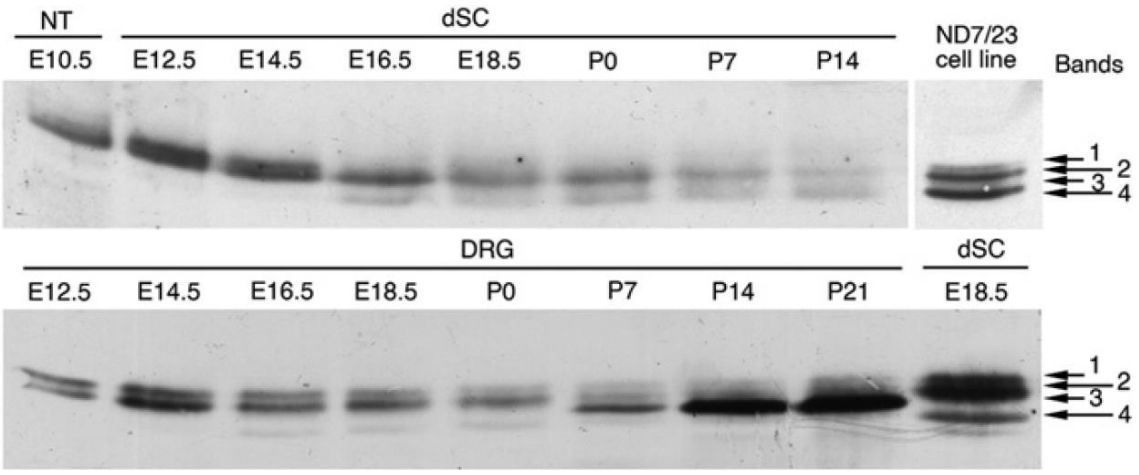

***Figure 9* - Prrxl1 band patterns in dSC and DRG throughout development**. Aside from being age-specific, Prrxl1 phosphorylation also appears to be site-specific, since DRG and dSC patters are distinct when considering different developmental ages (as seen for example in E16.5). Later developmental stages appear to display lower bands overall, which indicates dephosphorylation of Prrxl1. ND7/23 cells Prrxl1 band patterning appears to correspond to that of P0 dSC (Soares-dos-Reis et al., 2014).

1.7 S119A phospho-defective mutant

By combining large-scale immunoprecipitation with mass spectrometry analysis, multiple Prrxl1 phosphorylation sites were identified (Soares-Dos-Reis et al., 2017; Soares-dos-Reis et al., 2014). Each phospho-sites were mutated, either to aspartate, thus mimicking constitutive phosphorylation, or, alternatively, to alanine, which impaired phosphorylation at the site. These Prrxl1 phosphorylation mutants, when overexpressed in ND7/23 cells, present distinct transcriptional activity (Figure 10A) and electrophoretic mobility (Figure 10B). The impairment of the phosphorylation at S119 (serine replaced by alanine - S119A) causes the most drastic effects in terms of loss of Prrxl1 transcriptional activity, as seen in Figure 10A *(Soares-Dos-Reis et al., 2017)* and band pattern (Figure 10B).

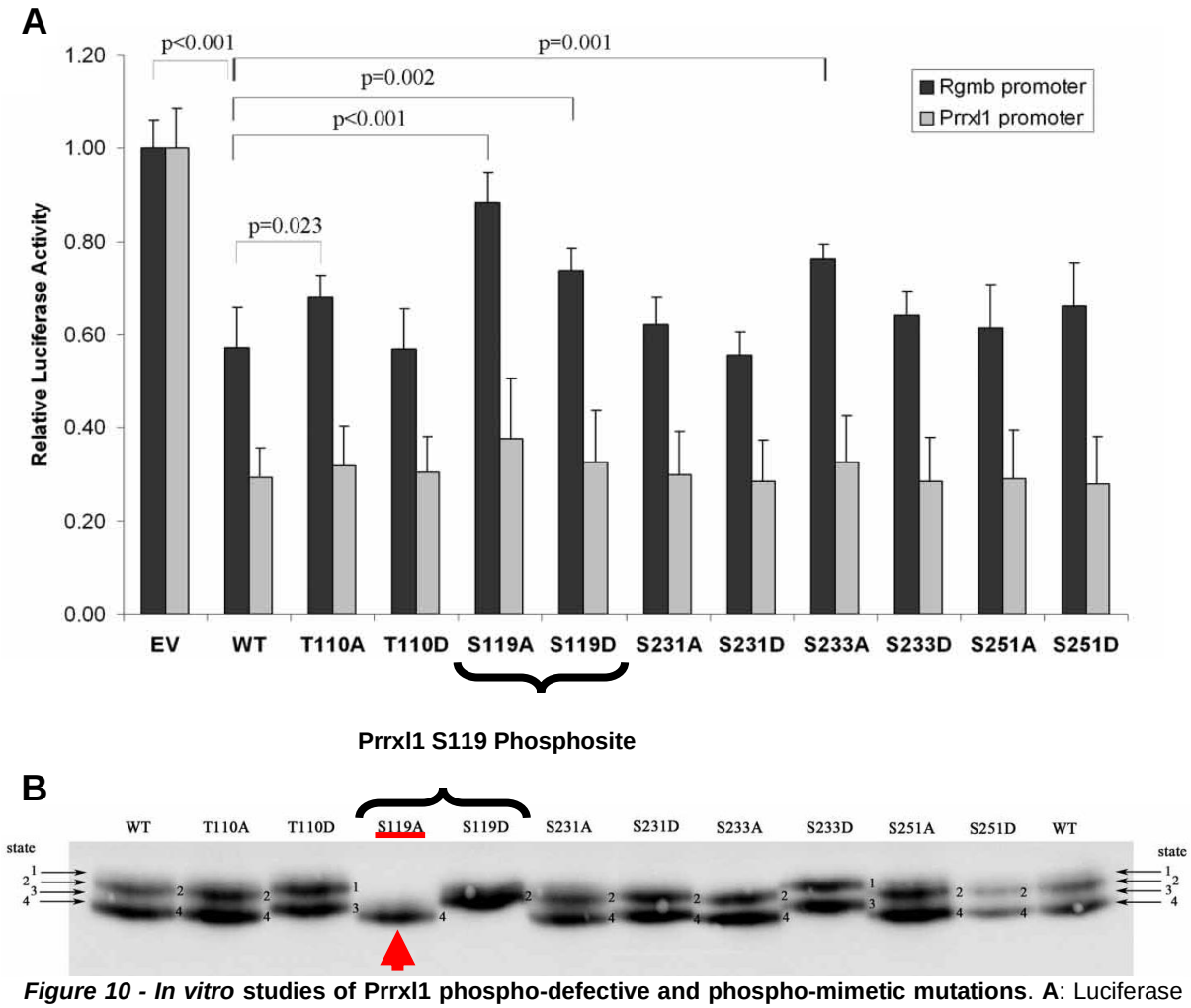

***Figure 10 - In vitro* studies of Prrxl1 phospho-defective and phospho-mimetic mutations**. **A**: Luciferase reporter assay indicative of Prrxl1 mutant transcriptional activity on both the Rgmb and Prrxl1 promoters. The Rgmb promoter is repressed by Prrxl1. In S119A, the activity of this promoter displays a higher value than in all other analysed mutations, which indicates that Prrxl1 transcriptional activity loss is greater in S119A mutants. Prrxl1 promoter activity remains constant throughout wild-type and analysed mutations, which suggest that phosphorylation does not play a role in Prrxl1 self-regulation; **B**: Western blot of wild-type and mutant variants, displaying the characteristic Prrxl1 band patterns. In S119A mutants, where phosphorylation of the S119 site is blocked, the single band corresponds to state 4. S119D mutants (which mimics constitutive phosphorylation) also display a single band but corresponding to state 2. Wild-type animals possess a pair of bands corresponding to states 2 and 4 (adapted from Soares-Dos-Reis et al. (2017).

While in these cells, wild-type Prrxl1 displayed a pair of bands, corresponding to states 2 and 4, S119 mutants only retained one of those bands: constitutively phosphorylated mutant (S119D) had a band correspondent to state 2, while phospho-deficient S119A mutant exhibited the band associated with state 4 (Figure 10B) (Soares-dos-Reis et al., 2014). Thus, phosphorylation at the S119 site is responsible for state 2 band profile, and alterations at this site impact both on Prrxl1 conformation and transcriptional activity.

Importantly, these data also indicate that distinct promoters are differently affected by phosphorylation. In the specific case of Figure 10A, while the activity of the Rgmb promoter is clearly affected by S119 phosphorylation, Prrxl1 promoter appears to be unaffected by the presence or absence of phosphorylation at that site, as well as at other sites equally studied (Figure 10A). These results seem to point toward gene-dependent regulatory functions of Prrxl1 phosphorylation, allowing it to behave differently depending on the gene promoter it is targeting or acting upon (Soares-Dos-Reis et al., 2017).

1.8 Prrxl1^{S119A} mouse model

For the study of Prrxl1^{S119A} phospho-defective mutation, a knock-in mouse mutant was produced by the genetically modified mouse unit, at i3S, using the CRISPR-Cas9 genetic editing technology. The alterations consisted in the substitution of a total of four bases, in three consecutive codons: two in the first codon, which caused the amino-acid substitution of serine-119 by an alanine, while the following base substitutions occurred in the two subsequent codons (Figure 11). While the conversion of a serine to an alanine allowed for a constitutive dephosphorylation at the 119 site, the last two base alterations (which did not alter any amino-acids) provided a recognition site for specific enzymatic digestion, therefore facilitating genotyping through RFLP (further approached in the *Mouse model validation* section of *Results*). The generation of this mutant mouse created the perfect model to test the in vivo implications of losing S119 phosphorylation. Since no *in vivo* studies have been conducted using this mutant mouse, a full characterization must be done, as well as a comparison with data the already obtained with Prrxl1 constitutive knock-out mice.

WT allele										
V	R	N	I	N	S	P	P	P	G	D
GTG	AGG	AAC	ATC	AAC	TCT	CCA	CCC	CCA	GGG	GAC

S119A allele										
V	R	N	I	N	**A**	P	P	P	G	D
GTG	AGG	AAC	ATC	AAC	**G**C**C**	CC**T**	CC**A**	CCA	GGG	GAC

***Figure 11* - Comparison between the wild type allele and the one harbouring the S119A mutation**. In total, 4 bases in three codons are substituted. However, due to the redundant nature of the genetic code, only one amino-acid is altered (S119 becomes an Alanine). The introduction of these silent mutations originates a restriction site crucial for animal genotyping.

1.9 Goals

With this work we aim to characterize the S119A phospho-defective mutation and unveil its functional impact on the development of nociceptive neurons. To achieve this, we aim to:

1) validate the knock-in Prrxl1^{S119A} phospho-defective mutant by optimizing a genotyping protocol and confirm the change in Prrxl1 electrophoretic mobility pattern;
2) identify possible morphological abnormalities present in the DRG/dorsal spinal cord of Prrxl1^{S119A} mice by using markers for primary afferent innervations and neuronal populations;
3) study the impact of S119 defective phosphorylation in the Prrxl1 transcriptional activity by evaluating putative changes in gene expression of selected Prrxl1 targets;
4) study to what extent the lack of phosphorylation at S119 impacts on the synaptic transmission of noxious stimuli from DRG to spinal cord.

CHAPTER 2

METHODS

2.1 Animal housing

Animals were housed and maintained at the i3S Animal Facility.

Two separate lines of both wild-type and Prrxl1^{S119A} phospho-defective mutant animals were kept as to avoid the need for genotyping every animal. All experiments complied with European Community Council Directive (86/609/EEC).

2.2 Genotyping

Samples were collected from new-born mice before weaning at the i3S Animal Facility.

DNA was extracted via cellular lysis by treating the sample with NaOH 1M and heating to 99 ºC for 15 minutes. pH of samples was corrected using 1M Tris-HCl.

Strategy I was then used to genotype the samples. Polymerase Chain Reaction was performed using a set of two primers (Forward: 5'-GCTGGAAGGTGGAGTGTGTC-3'; and Reverse: 5'-CAGAGCTACCCCAGACTCCT-3'), flanking the S119 site. NZYTaq II DNA Polymerase (*nzytech*) was used and the reaction was executed according to protocol. Primer annealing temperature was optimised to 62 ºC. The resulting fragment had a total of 597 base pairs (bp). Genetic editing at the S119 site through CRISPR-Cas9 not only altered an amino-acid (Serine to Alanine, for constitutive dephosphorylation of the 119 site), but also changed two bases in the following two triplets, establishing a recognition site for *EcoNI* (or *XagI*) in the S119A allele. The samples were then purified through isopropanol/ethanol purification, to further the efficiency of the restriction enzyme. Through *Restriction Fragment Length Polymorphism* (RFLP), the samples were digested during 7 hours at 37 ºC, using 0,5µL of *EcoNI* (values optimized for complete digestion in the S119A mutant). The two obtained fragments varied in size: one had 502 bp, while the other had 95 bp. This difference in length made it possible to identify the genotype of each sample after 2% agarose gel electrophoresis, in which the wild-types had only a band around the 600 bp, the heterozygous had two bands, one near 600 bp, and the other near 500 bp, and lastly, the homozygous S119A mutant presented a single band near 500 bp. This ~500 bp band was the result of *EcoNI* digestion of the initial ~600 bp fragment, which in the Wt/S119A produced a ~600 bp band (corresponding to the wild-type allele) and a ~500 bp band (corresponding to the S119A allele), and in the S119A/S119A resulted in a single ~500 bp band (corresponding to the only type of allele present, the S119A). Furthermore, a ~100 bp band was also present if digestion occurred but was not necessary to assess the genotype of each sample.

Results of homozygous lines founders were further confirmed through Sanger sequencing to verify the presence of the mutation at the S119 site.

2.3 Tissue harvesting

Animals were sacrificed through cervical dislocation and the embryos (E13.5 and E14.5) were surgically removed.

Spinal Cords (SCs) and Dorsal Root Ganglia (DRGs) of both *wild-type* and Prrxl1^{S119A} phospho-mutants were collected. SCs were separated into ventral and dorsal portions and stored separately, and DRGs were stored in pools of two animals to increase the RNA yield after extraction.

Tissues used for gene expression analysis (real time PCR) were suspended in TRIzol Reagent (*Invitrogen*) and stored at -80 ºC. Tissues used for protein analysis were stored directly at -80 ºC. For histologic processing, the whole embryo was collected.

2.4 Histology

After being surgically removed, embryos were fixed in 4% paraformaldehyde in PBS (phosphate-buffered saline) solution for 24 hours, the embryos were thoroughly washed with PBS and resuspended in 30% sucrose in PBS solution. This solution was replaced with fresh 30% sucrose in PBS solution after the embryo had sunk to the bottom of the tube. After this, tissues were embedded in Optimal Cutting Temperature (OCT) embedding matrix (*Kaltek*), sectioned in a cryostat microtome, placed in microscope positive charged slides (*APTACA*) and stored at -80 ºC.

2.5 Immunohistochemistry

Immunohistochemistry (IHC) was utilized in this work to study neuronal populations and fibre innervation alike.

Slides were heated to 50 ºC for 20 minutes and placed in PBS for another 20 minutes. After washing with PBS 0,1 % Tween-20, endogenous peroxidase was blocked using 4 % H_2O_2. This step was performed to avoid background upon chromogenic detection using DAB (discussed ahead). Membranes were then permeabilized using PBS 1% Triton X-100 10% BSA for 3 minutes, and proteins were blocked using PBS 0,1% Tween 10% BSA for one hour, followed by primary antibody (diluted in PBS 0,1% Tween 2 % BSA) incubation

overnight in a wet chamber. Utilized primary antibodies are presented in Table 1, as well as the concentrations used.

Table 1
Primary antibodies (IHC)

Antibody	Production	Concentration	Type
α-TrkA *(R&D Biosystems)*	Goat	1:1000	Fibre marker
α-TrkB *(R&D Biosystems)*	Goat	1:500	Fibre marker
α-Prrxl1 *(homemade)*	Rabbit	1:500	Population marker
α-Tlx3 *(Santa Cruz Biotech)*	Rabbit	1:100	Population marker

The following day, slides were washed using PBS 0,1% Tween-20 and were incubated for one hour using secondary antibody diluted in PBS 0,1% Tween 2% BSA. Utilized secondary antibodies are presented in Table 2, as well as respective use concentrations.

Table 2
Secondary antibodies (IHC)

Antibody	Conjugate	Concentration
α-Rabbit *(Santa Cruz Biotech)*	Biotin	1:200
α-Goat *(Jackson Immunoresearch)*	HRP	1:200

For incubations with biotinylated secondary antibodies, slides were once again washed in PBS 0,1% Tween-20 and incubated for one our using ABC (avidin-biotin complex - *Vector Laboratories*) (1:200). Slides were washed using the same washing solution and then revealed with 3,-3'diaminobenzidine (DAB, substrate to HRP) (2,5 mg DAB in 0,05M Tris-HCl in H_2O), originating a brown product as DAB is converted by HRP (approximately 30 minutes, but varied depending on the antibodies used). Slides incubated with HRP (Horseradish Peroxidase)-conjugated secondary antibodies were washed in PBS 0,1% Tween-20 (following incubation) and then revealed with DAB, jumping the ABC incubation. All slides were washed with PBS after DAB incubation and left to dry overnight at 37 ºC. Following this, slides were hydrated and briefly counterstained with haematoxylin to provide a slight blue/purple contrast to the finished product. Slides were dehydrated after staining and mounted with a coverslip using Eukit mounting medium (*Sigma-Aldrich*).

2.6 Gene expression analysis

Spinal cord (dorsal portion) and Dorsal Root Ganglia (DRGs) samples were collected from both wild-type and S119A phospho-mutant mice, suspended in TRIzol®Reagent (*Invitrogen*) and stored at -80 ºC.

Samples were later processed, and RNA was extracted using NZY Total RNA isolation kit (*NZYTech*) according to its specifications. To check for RNA concentration within each sample, NanoDrop™2000 Spectrophotometer (*Thermo Scientific*). 1 µg of RNA was then used to synthetized cDNA utilizing the NZY First-Strand cDNA Synthesis Kit (*NZYTech*) according to its specifications. After cDNA synthesis, all leftover RNA was eliminated using RNAse H (*NZYTech*). cDNA samples were used to quantify genes of interest expression using StepOnePlus Real-Time PCR system (*Applied Biosystems*) along with PowerUp™SYBR Green Master Mix (*Applied Biosystems*). Normalization was done through amplification of HPRT and GAPDH. Primers (sense and anti-sense) used are presented in Table 3.

Table 3
qPCR primers

Gene	Sense Primer (5'→3')	Anti-sense Primer (5'→3')
Cck	GCGATACATCCAGCAGGTC	TCCATCCAGCCCATGTAGTC
Galrl	TACCTTTCTGCCCTTACTGCTC	ATACTACAACGACCACCACCAGGA
Grik3	TTTGGAATGGGCTCCCTGAT	GAGGGTGAAGAACCACCAGA
Tlx3	GGTTCCAAAAGAGGAC	ACGAGTTGTGCAGAGC
Kirrel	GTGTGCCATCAATATG	CTCATACACGCATCCT
Cdh22	TGATGCAGACCTACTT	GGCTTGAATACCTCGT
Sema3e	ATTCCCTGAAGAACGA	TGTGGATCAATCCAGT
Pdm11a	TCGGATGGTTACCACA	CCCACAATCATAAAAT
Whrn	GGGGACCACACAGAAGAAGG	TGGCTTGGTCGTCCAGCAGT
Ccdc68	AAGCGCCGAAAGTCTGAATC	CAGCGTTGGATTTAAGCTGG
Pcdh11x	CTTTCAAGGCCCCTGTGTCT	CAGATCGCCGCTGTGGAT
Lmo3	CATGAGGACTGAAGTG	CAGGGATGAGCTACAG
Dach2	CCTAAGCGTTGGGAGT	CATTTTGGCTTTACCC
Bcn2	CCAGACTGGCAAGCACATTT	CCCTCTTTGGCTCTCTGTCT
Htr3a	CTGCACACCATCCAGGACAT	CGGCGGATGATCACGTAGAA
Vav3	GTGGCTCATCCACAGCAAGG	TCTTCAAACAGAGAAACTGGGACA
Rasgrp	GTGTTCGAGTGCAAGAAGCG	ATCCTTCTTCGGGTGCATGG
Npffr2	CTGGCTAGGATGGCGAATGG	GCTCATGGTGGACCTTCCTAA
Grla2	CCTCGCAGACCCTATCTCCT	TTCACTCGGTAGTCCATGGTG

2.7 Protein extraction

Samples were suspended in 1 mL of PBS with 0,1% Triton X-100, supplemented with 1% protease and phosphatase inhibitors. Homogenization was achieved using MagNA Lyser (*Roche*) and then sonicated in Bioruptor UCD-200 (*Diagenode*) for ten minutes and cleared through centrifugation.

Proteic quantification was calculated using the Bradford protein assay (1 µL of proteic extract in 99 µL of Bradford reagent, in triplicates). Signal was read at 595 nm using Infinite 2000 spectrophotometer (*Tecan*). Concentration values were obtained utilizing a BSA calibration curve.

2.8 Western blot

After protein extraction, proteic extract correspondent to the desired amount of protein (typically 20 µg) was diluted in Gel Loading Buffer (50mM Tris, pH 8.8, 2% SDS, 10% glycerol, 0,2% bromophenol blue supplemented with fresh 2% DTT).

Samples were heated to 50 ºC for 20 minutes and centrifuged to pull any residues toward the bottom of the tube. Samples were then loaded into a 12% SDS-polyacrylamide gel and ran at 30 mA. The gel was then blotted into a nitrocellulose membrane using the Trans-Blot Turbo RTA Transfer Kit (*BIORAD*) and respective equipment. The membrane was temporarily stained with Ponceau S to assess if calibration between wells had been properly achieved. After removing this stain from the membrane, we proceeded with blocking it in a TBS 0,1% Triton X-100 5% non-fat milk for 1 hour. After the protein block was completed, the membrane was incubated overnight in orbital shaker with primary antibody diluted in TBS 0,1% Triton X-100 2% non-fat milk. The antibodies and respective concentrations of use are represented in Table 4.

Table 4
Primary antibodies (WB)

Antibody	Production	Concentration
Prrxl1 *(homemade)*	Rabbit	1:500
cFos (*CellSignaling*)	Rabbit	1:1000
α-Tubulin *(Sigma-Aldrich)*	Mouse	1:10000

The next day, the membrane was washed thoroughly and then incubated with the secondary antibody, diluted in TBS 0,1% Triton X-100 2% non-fat milk. The various used antibodies and their respective concentrations of use are presented below, in Table 5.

Table 5
Secondary antibodies (WB)

Antibody	Conjugate	Concentration
α-Rabbit *(BIORAD)*	Fluorescent*	1:10000
α-Rabbit *(Jackson Immunoresearch)*	HRP	1:10000
α-Mouse *(Jackson Immunoresearch)*	HRP	1:10000

* - α-rabbit IgG StarBright Blue 700

After this, the membrane was thoroughly washed once again with TBS 0,1% Tween-20 several times. When using HRP-conjugated secondary antibodies, the Clarity Western ECL substrate (*BIORAD*) was used according to its protocol. ChemiDoc MP Imager (*BIORAD*) was used to reveal and capture images of both HRP secondary- as well as fluorescent antibodies, using appropriate light settings and exposures.

2.9 Formalin test and fresh spinal cord dissection

The protocol we performed was based in previous works involving a formalin test in mice or rats (Dubuisson & Dennis, 1977; Gong et al., 2014; Hunskaar, Fasmer, & Hole, 1985; Murray, Porreca, & Cowan, 1988). 12 mice were places in the testing room overnight to allow for them to adapt to the environment. Prior to the injection, all mice were lightly anesthetised using isoflurane. We performed a plantar subcutaneous injection of 15 µL at the right hind paw. The injected substance depended on the condition (see Table 6).

Table 6
Formalin test

Injected Solution	Conditions			
	Test		Sham	
Composition	3 Wild types	3 Prrxl1^{S119A}	3 Wild types	3 Prrxl1^{S119A}
5% Formalin	Yes	Yes	No	No
Saline	Yes	Yes	Yes	Yes

A 5% formalin (from a stock 37% formaldehyde solution) in saline (0,9% NaCl) was injected in a total of 6 animals (the test animals, as seen in Table 6), while the other 6 only received saline (sham test). This last 6 mice served as controls for both the wild-types and Prrxl1^{S119A} mice. After this, we waited 2 hours to sacrifice the animals. The L4-L5 segment of the dorsal column was removed, and the spinal retrieved. After this, we separated the ipsi- from the contralateral side (ipsilateral being the left side of the spinal cord, opposed to the injected right hind paw). Samples were adequately labelled and stored at -80 ºC for later protein extraction.

2.10 Statistical analysis

Student's t test (two-tailed, unpaired) was used, and the P values indicated result from at least three independent experiments.

Analysis and graphics were made using Microsoft Excel 2016 along with GraphPad Prism 8.

CHAPTER 3

RESULTS

3.1 Mouse model validation

3.1.1 Establishment of a genotyping method

A knock-in mouse model harbouring the Prrxl1^{S119A} mutation was produced by the i3S transgenic mouse facility, by using CRISPR-Cas9 genome editing. Besides the substitution of TCT (serine codon) to GCC (alanine codon), the approach was designed in such a way that an *EcoNI* recognition site was inserted allowing the use of *Restriction Fragments Length Polymorphism* (RFLP) as a genotyping method (Figure 12). After PCR, the DNA amplicon is digested by *EcoNI* originating two fragments of 502 and 95 base pairs, in the case one allele contains the polymorphisms. The presence of the fragments is identified by 2% agarose gel electrophoresis. To further enhance the restriction reaction, the samples are purified after PCR. Note that the restriction enzyme does not recognize the DNA site corresponding to S119. Thus, we will assume that *EcoNI* digestion, due to insertion of the two nearby polymorphisms, also means substitutions in the S119 site.

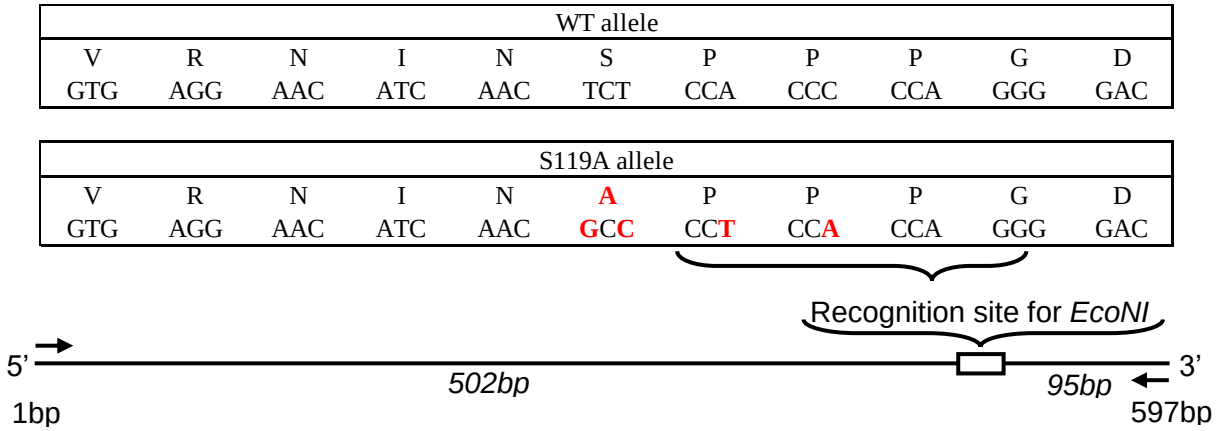

***Figure 12*- Genotyping strategy**. Comparison between the wild-type and S119A alleles and diagram of Strategy I-resulting amplified fragment. Recognition site of EcoNI is also highlighted in both the S119A allele and the fragment diagram. In total, 4 altered bases result in the alteration of an amino-acid (Serine to Alanine), which constitutively impairs the phosphorylation at the site, and the introduction of a recognition site for EcoNI, which allows for the fragment to be cut and facilitates genotyping. After digestion with EcoNI, two fragments of 502 and 95 base pairs are obtained.

Another genotyping approach was designed by the i3S transgenic mouse facility, termed Strategy II, and consisted in the use of three primers: a *forward primer*, common for both the wild-type and S119A alleles, and two *reverse primers*, each of them being specific for one of the two alleles, thus differentiating between the two genotypes. After some optimization of the PCR condition, we concluded that this strategy is prone to primer mispairing and decided to use Strategy I to genotype mouse samples from here on after.

As a result of CRISPR-Cas9 gene editing manipulation, several animals were obtained. From those, three mice (#4, #13 and #21) were genotyped by RFLP. The genotyping results, as seen in Figure 13A, show the presence of one wild-type (#4) and two heterozygous animals (#13 and 21). Animal #4 presents a single ~600bp band after digestion, which indicates the presence of two wild-type alleles. Animals #13 and #21 displayed two bands of ~600 and ~500 bp. This indicates the presence of one wild-type allele and a S119A allele and therefore could be characterized as heterozygotes. Worth mentioning is the fact that the 95 bp fragment that is generated upon digestion does not appear in these images due to its low molecular weight. Regardless, the presence of the 502 bp band is sufficient to genotype the sample.

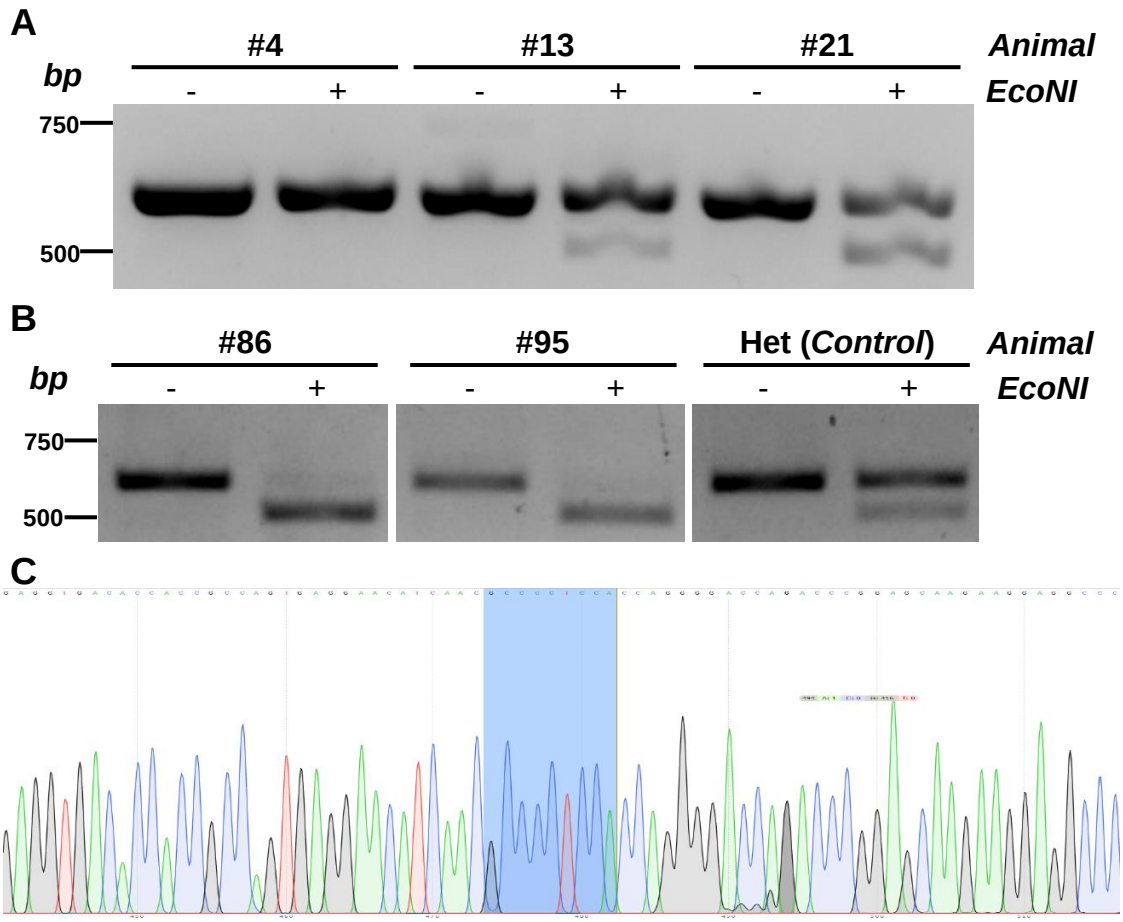

***Figure 13* - Genotyping and sequencing results**. **A**: Electrophoretic analysis of samples #4, #13 and #21. EcoNI digestion creates a new band, which allows for the correct genotyping of each sample. In #4, the digested and non-digested samples appear similar, which indicates the presence of two wild-type alleles, which are not cut by EcoNI. In #13, digestion occurred but the upper band was still present, what hints toward the presence of two different alleles, a wild-type and a S119A allele. Samples #21 corresponds to the first CRISPR-Cas9 -generated mouse. However, it appears in the gel with both the upper (Wt) and lower (S119A) band present; **B**: Genotyping results of the first S119A mutant mice compared to a heterozygous control. The complete digestion of the upper Prrxl1 band can be clearly seen in samples #86 and #95, which indicates the presence of two S119A Prrxl1 alleles in these animals; **C**: Sanger sequencing of animal #86. To guarantee the accuracy of our genotyping results, Sanger Sequencing was performed, which allowed us to verify that the animal was indeed a homozygous mutant.

We chose the animal #21 as the founder of the colony. To stabilize the mutation and expand the line, this animal was crossed with a wild-type mouse and the heterozygous progeny were further mated with wild-type mice. This procedure was repeated six times, generating enough animals in the colony to start with the production of phospho-mutant homozygotes. An example of genotyping of those animals (mice #86 and #95) is presented in Figure 13B. For both animals, a single ~500 bp band was present, confirming that only the S119A allele was present. These results were further confirmed through Sanger sequencing (Figure 13C). Unlike the Prrxl1-null mutant mice, these animals did not present an observable phenotype, displaying normal life expectancy, normal size/weight, and no visible abnormalities (Figure 14).

***Figure 14* - Prrxl1^{S119A} and wild-type side-by-side comparison**. The white arrow indicates the phospho-defective mutant mouse, while the one with the painted tale is the wild-type. No visible abnormalities, such as difference in size are visible between these two animals. In Prrxl1 constitutive knock-out, however, the mutant was considerably smaller and presented fur lesions just above the tail. Their life expectancy was also severely reduced when compared to wild-types (Chen et al., 2001).

3.1.2 Prrxl1^{S119A} protein displays an electrophoretic mobility shift *in vivo*

In previously published studies (Soares-Dos-Reis et al., 2017; Soares-dos-Reis et al., 2014), the Prrxl1^{S119A} protein presents a specific electrophoretic motility profile when overexpressed in neuronal cell cultures. This pattern was seen by SDS-PAGE as a slightly faster migration, resulting in an electrophoretic shift when compared to its wild-type counterpart (see figure 10B in introduction section). This alteration in the migration pattern was attributed to conformational changes associated with the lack of phosphorylation at the S119 site (Soares-dos-Reis et al., 2014). Our *in vivo* approach also revealed the same shift in the migration pattern of S119A Prrxl1, as observed by western-blotting analysis of spinal cord protein extracts from wild-type and Prrxl1^{S119A} E13.5 embryos (Figure 15).

This indicates that the Prrxl1^{S119A} mouse reproduces some of the alterations previously reported in neuronal cell line and thereby validates this animal model.

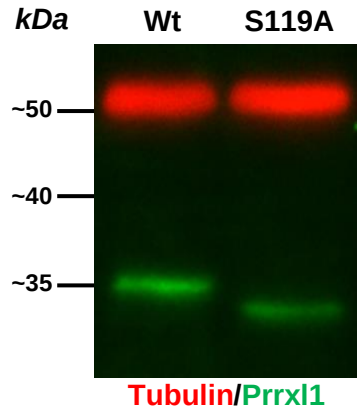

***Figure 15* - Electrophoretic motility shift of Prrxl1^{S119A}**. Western blot analysis of Prrxl1 wild-type and S119A mutant mice, along with tubulin loading control. An electrophoretic shift can be discerned, as indicated by the white arrows. S119A Prrxl1 appears to migrate slower across the gel, which hints toward phosphorylation-dependent conformational changes, which affect the electrophoretic motility

3.2 Selected Prrxl1 target gene expression analysis

We considered the possibility of gene expression being affected by the presence of the S119A phospho-mutation. Since Prrxl1 is a transcription factor, its activity influences the expression levels of its targets. In Prrxl1 specific case, this target expression modulation mainly occurs during embryonic stages, where it is important for the accurate development of the nociceptive system (Chen et al., 2001). As previously mentioned, the control of Prrxl1 transcriptional role occurs in a variety of ways, one being through phosphorylation. Previous studies revealed that its phosphorylation state varies in an age- and tissue-dependent manner (Soares-dos-Reis et al., 2014), suffering a gradual dephosphorylation as development progresses. Later, studies performed in neuronal cell line identified that S119A mutation clearly impacts on Prrxl1 transcriptional activity, inducing changes in target gene expression (Soares-Dos-Reis et al., 2017). Being aware of this, we decided to test if, using our Prrxl1^{S119A} mouse model, we could detect variations in Prrxl1 targets gene expression levels that could be traced to the lack of phosphorylation at the S119 site. For this analysis, we used two distinct developmental timepoints, E13.5 and E14.5, which are temporally located between the end of neurogenesis and the cellular death reported in Prrxl1-null mice, which occurs around embryonic day 17 (Chen et al., 2001). Although we still have not analysed the occurrence of putative cell death in Prrxl1^{S119A} spinal cords, the selected developmental ages allow us to study the neuronal populations impacted by Prrxl1^{S119A} mutation avoiding any possible effects originated by eventual neuronal loss.

To determine the best candidates, we first tested Prrxl1 direct targets that had a greater expression variation in Prrxl1-null mice when compared to wild-type counterparts. These data had previously been obtained through a dataset generated by the combination of ChIP-seq and microarray approach in E14.5 spinal cord and dorsal root ganglia samples (Monteiro, unpublished). We began our experiments evaluating Prrxl1 targets expression in E13.5 wild-type and Prrxl1^{S119A} mouse embryos through qPCR of genes that had scored significant expression variations (<0,6 and >1,4 fold change) in the above dataset. For this first approach, the RNA samples were extracted and pooled into groups (2 samples per group) according to their tissue (dorsal SC or DRG) and genotype (Wt or S119A). As seen in Figure 16, the possible variations detected through qPCR were almost always inferior and sometimes did not correspond to those previously detected in Prrxl1-null tissues. However, some differences in gene expression were observed as for the case of GALR1 and TLX3 in SC, and CCK, WHRN, CHODI, CCDC68 in DRG.

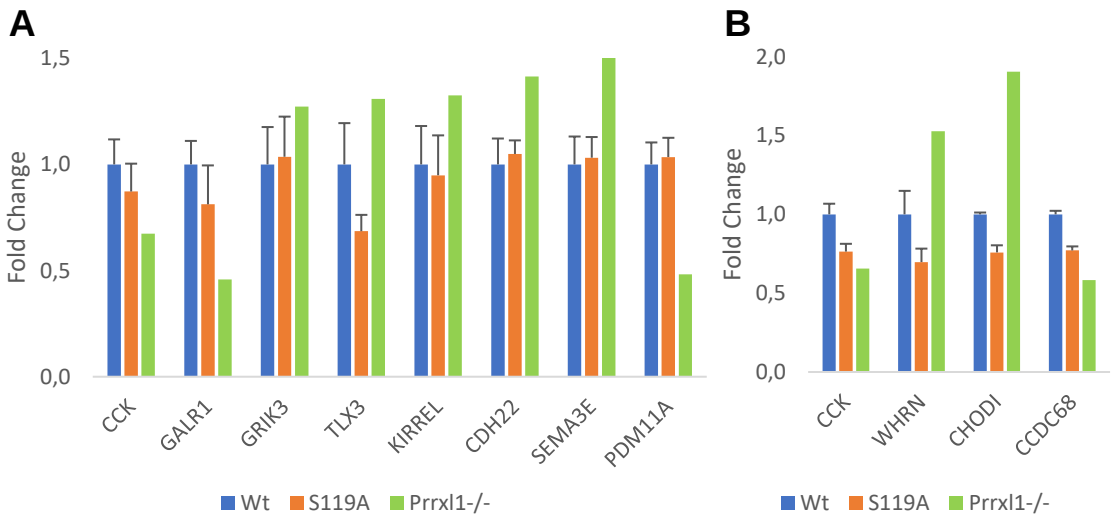

***Figure 16* - Prrxl1 targets expression in E13.5 dSC and DRG (I)**.Prrxl1 targets expression fold change in **A**: dorsal spinal cord; and **B**: dorsal root ganglia. For this test, samples were pooled to dilute possible outliers, thus allowing a broader first approach. Values obtained from Prrxl1 mutants (orange) normalized according to wild-types (blue). The values obtained by Monteiro (unpublished) are also presented for comparison (green).

From these results, we selected those targets which appeared to be the most promising and repeated the qPCR analysis increasing the number of animals in our analysis. Spinal cord samples were processed individually, while DRG samples were instead pooled into groups of two with the intent of increasing RNA concentration. The results are presented in Figure 17. In the E13.5 dSC, no major or statistically significant differences appear to be present. However, a huge dispersion between wild-type samples were observed, which

strongly interfered with the analysis. On the other hand, in E13.5 DRG, Prrxl1 targets CCK and CCDC68 appeared to be overexpressed in Prrxl1^{S119A} mutants. However, due to the low number of samples, no statistical analysis could be accurately performed. As previously mentioned, the DRG sample pooling into groups of two elements causes our total number of samples to be halved, which results in statistical significance issues. Despite this, a trend seems to be present. Also, worth mentioning is a somewhat marked variability in wild-type samples throughout both tissues in analysis.

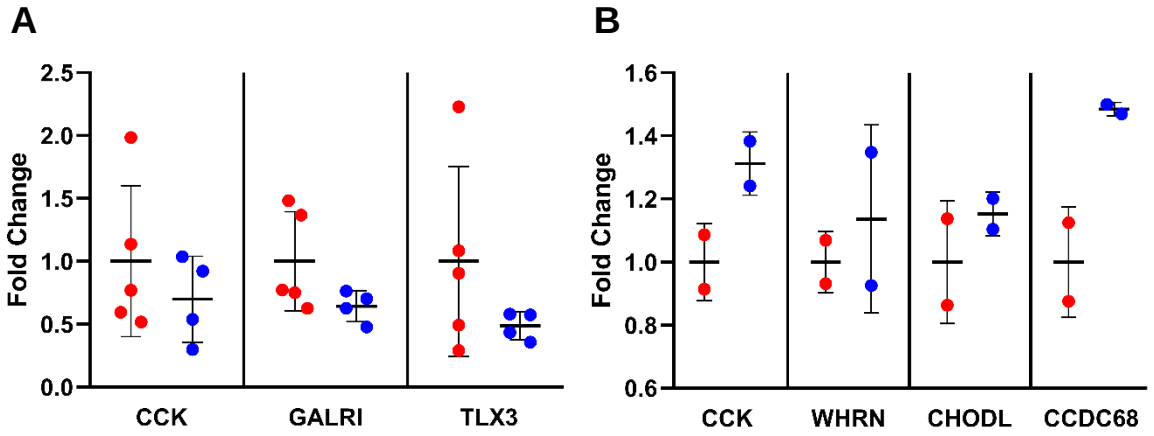

***Figure 17* - Prrxl1 targets expression in E13.5 dSC and DRG (II)**. Prrxl1 targets expression fold change in **A**: dorsal spinal cord; and **B**: dorsal root ganglia. DRG RNA samples were pooled into groups of two to increase RNA concentration. Wild-type: red; Prrxl1 S119A: blue.

To further assess if expression of Prrxl1 targets is impacted by the S119A phospho-mutation, we also analysed samples from E14.5 embryos. We decided to repeat targets with some degree of variation at E13.5 (CCK and CCDC68 in DRG samples), and test new possible candidates selected from the target list generated from E14.5 Prrx1-null embryos (Monteiro, unpublished). The results can be seen in Figure 18. In the spinal cord, no Prrxl1 targets appear to be significantly affected. There is some trend in an upregulation of LMO3 gene in Prrxl1^{S119A} samples but remains to be proved by increasing the number of samples. In the DRG, targets that had previously been flagged as promising candidates in terms of gene deregulation (CCK and CCDC68), display at this embryonic age distinct results: i) CCK exhibits only a slight increase in expression in Prrxl1^{S119A} DRG at E14.5 when compared to what was observed in E13.5 (Figure 17); ii) CCDC68 expression appears now to be repressed at E14.5 (Figure 18), as opposed to the increase in expression observed in E13.5 (Figure 17). Once again, a high variability within samples (represented by the error bars) seems to be present in some cases, especially in DRG tissue.

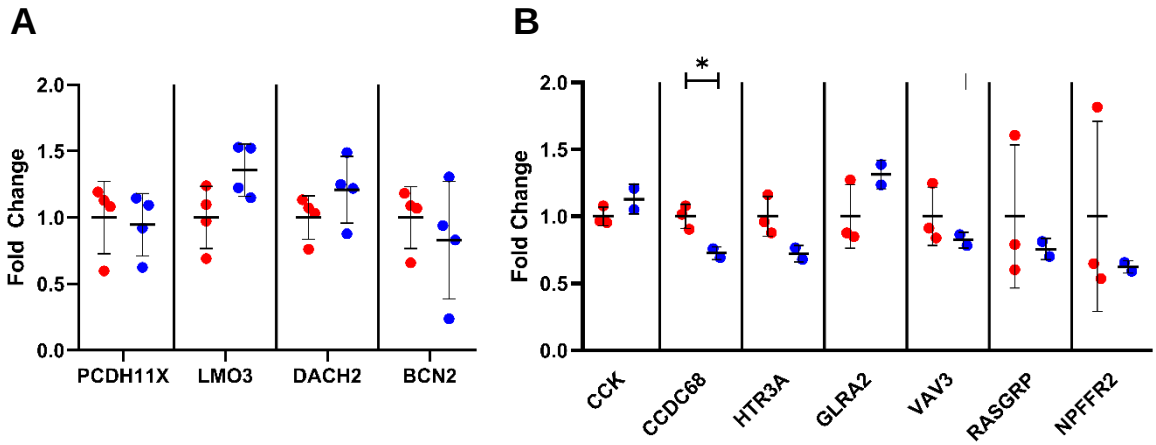

***Figure 18* - Prrxl1 targets expression in E14.5 dSC and DRG**. Prrxl1 targets expression fold change in **A**: dorsal spinal cord; and **B**: dorsal root ganglia. DRG RNA samples were pooled into groups of two to increase RNA amount. Wild-type: red; Prrxl1 S119A: blue.

3.3 Evaluation of putative morphological abnormalities in Prrx1^{S119A} spinal cords

Analysis of the morphology of the Prrxl1^{S119A} spinal cord, as well as the distribution of the various neuronal populations was accessed through immunohistochemistry as well as tissue stains.

3.3.1 Prrxl1^{S119A} does not impact on spinal cord morphology

The morphology of Prrxl1^{S119A} E13.5 spinal cord embryo was firstly assessed through thionine stain, providing us with a broad analysis of the overall spinal cord conformation. A phospho-mutant spinal cord was compared to its wild-type counterpart, allowing us to conclude that no major defects were present at the upper portion of the dorsal horn (lamina I to III), where expression of Prrxl1 occurs (Figure 19). In the spinal cord of Prrxl1 constitutive knock-out, no differences were observed at this age, since Prrxl1-dependent neurons death only began after embryonic day E17.5 (Chen et al., 2001).

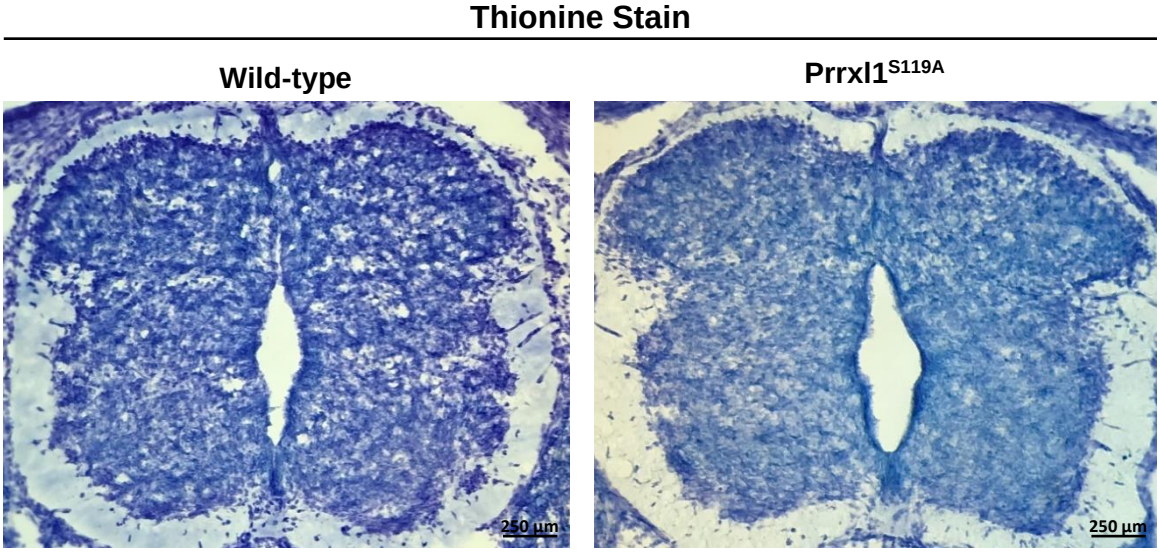

***Figure 19* - Thionine staining of wild-type and Prrxl1^{S119A} phospho-defective mutant E13.5 embryos**. No defects were detected in the spinal cord of the phospho-defective mutants when compared to its wild-type counterpart at embryonic day 13.5.

3.3.2 Prrxl1^{S119A} does not impact on spinal cord fibre innervation

At E13.5 afferent fibres, arising from DRG, penetrate the dorsal horn of the spinal cord, while at E14.5 significant ingrowth of such fibres occurred. In Prrxl1-null mice, afferent fibre projections are retarded and only enter the spinal cord at later stages (Chen et al., 2001). This delay caused marked morphological differences at these ages, since by E13.5, Prrxl1$^{-/-}$ mice afferent projections are still to invade the spinal cord, only starting to penetrate the dorsal horn after E14.5. We decided to assess if this delay also occurred in our Prrxl1^{S119A} knock-in mouse model. Consequently, we attempted to compare wild-type and Prrxl1^{S119A} mutants in terms of nociceptive afferent fibre innervation, using TrkA (specific to Aδ- and C-fibres). As previously mentioned, by E14.5, wild-type mice afferent fibres have already invaded the dorsal horn of the spinal cord. As seen in Figure 20, staining of afferent fibres is clear, both in the wild-type and Prrx1^{S119A}. The presence of TrkA^{+} neurons can also be seen in the DRG (Figure 20C and F). Furthermore, clear signs of fibre ingrowth in the most superficial regions of the dorsal horn can be discerned (Figure 20, white arrows). This ingrowth of fibres is detectable both in wild-type and in Prrxl1^{S119A} mice and is comparable in terms of fibre density and distribution. Thus, a delay in TrkA^{+} fibres innervation, previously detected on the Prrxl1-null mice (Chen et al., 2001), does not seem to be present in our phospho-defective mutant.

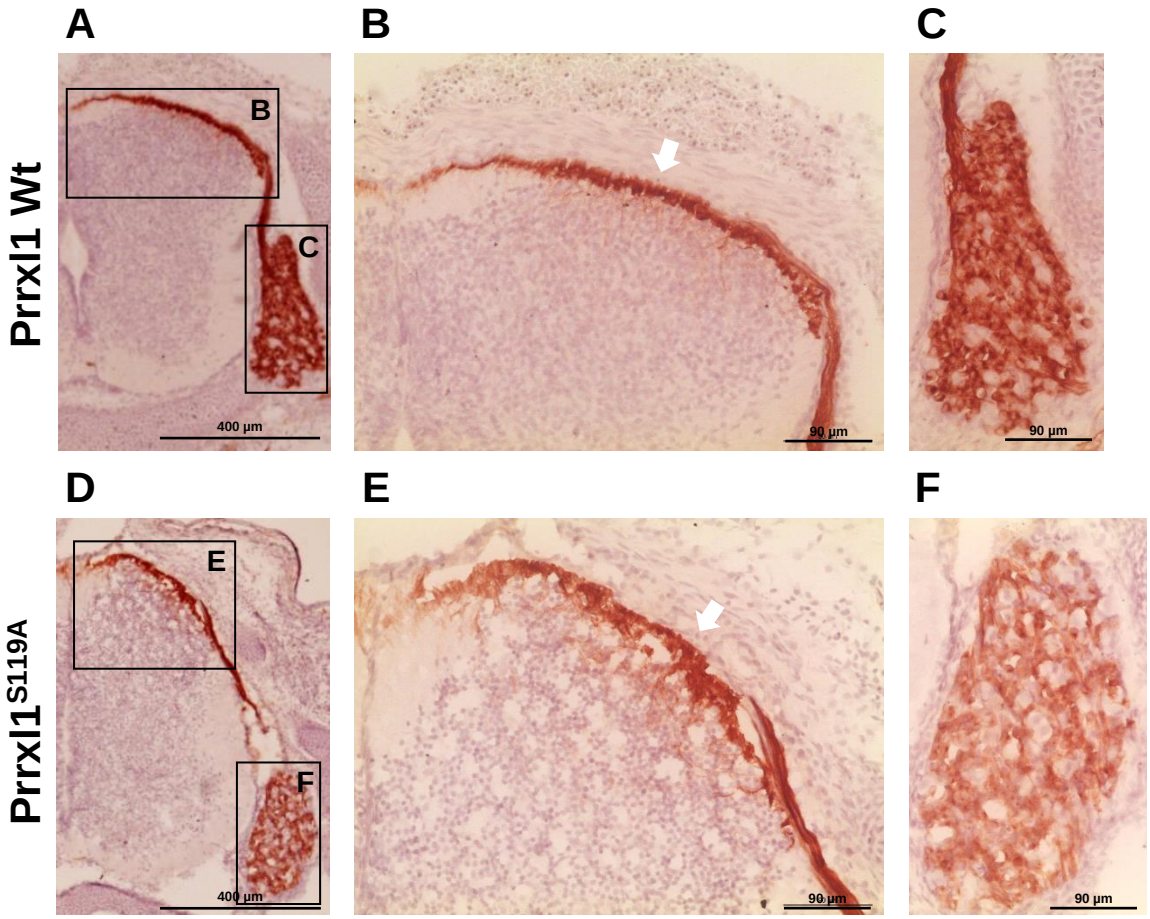

***Figure 20* - Anti-TrkA immunostaining of wild-type and Prrxl1^{S119A} phospho-defective mutant E14.5 embryos**. At this age, nociceptive afferents have already penetrated the dorsal horn of the spinal cord (white arrow, B and E) in both wild-type and phospho-mutant mice. This is a clear difference to the Prrxl1-null phenotype, where a significant TrkA$^+$ afferents innervation occurs, causing fibres to only start entering the dorsal horn at around E14.5. On both sides of the spinal cord, dorsal root ganglia (C and F) also appear stained due to the presence of TrkA$^+$ neurons. Haematoxylin counterstain is seen in purple.

We went on to assess if changes in other types of fibre, such as those positive for TrkC are observed (Figure 21). These types of fibres did not appear altered in Prrxl1-null mice (Chen et al., 2001), as the lack of Prrxl1 only seemed to impact on TrkA$^+$ fibres, responsible for carrying stimuli associated with nociception, in a time-specific manner. In our Prrxl1^{S119A} phospho-defective mutant, no alterations in fibre innervation were detected in E14.5 embryos when compared to wild-types, including in TrkC$^+$ fibres.

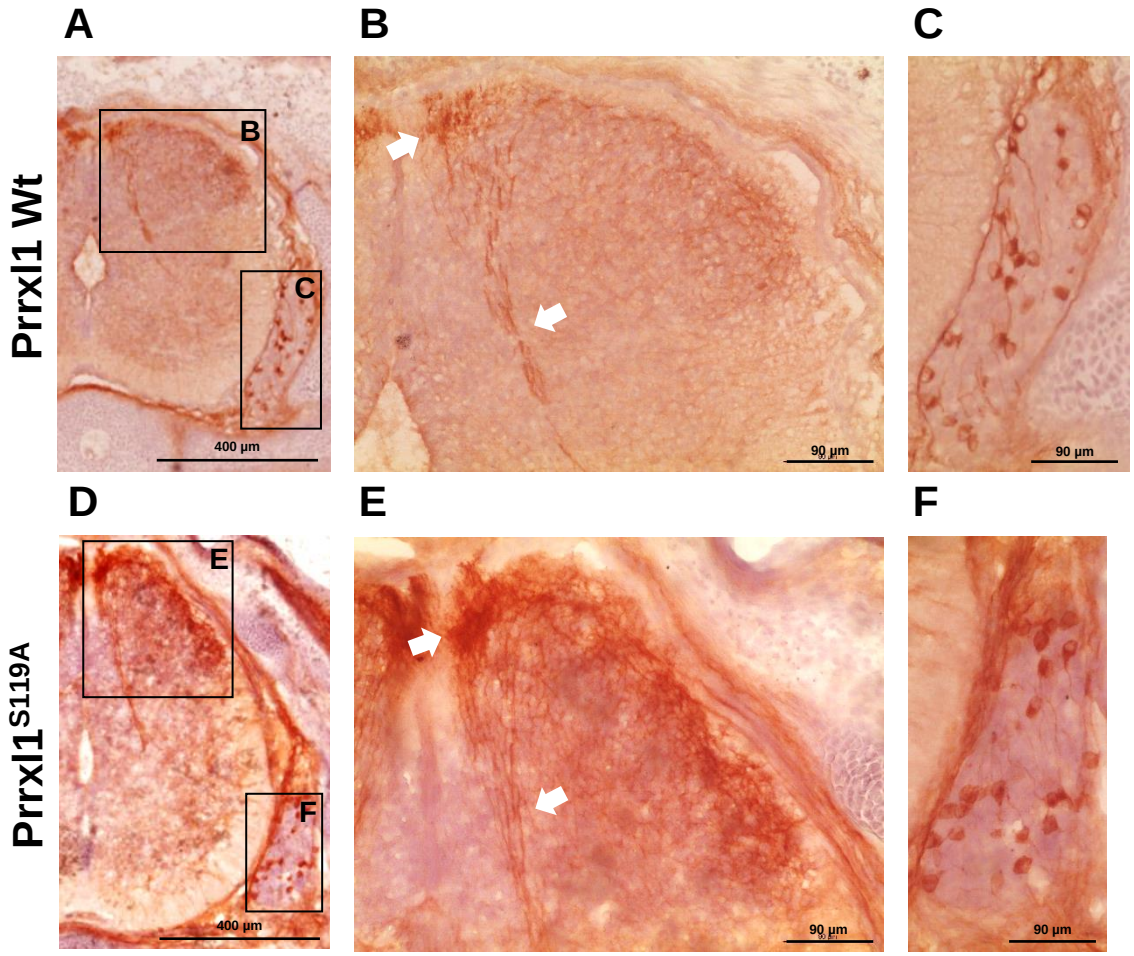

***Figure 21* - Anti-TrkC immunostaining of wild-type and Prrxl1^{S119A} phospho-defective mutant E14.5 embryos**. TrkC^{+} fibres tend to project to a region located in the medial aspect of lamina VII (Lai, Seal, & Johnson, 2016). The projections, indicated in both the wild-type and Prrxl1^{S119A} with a white arrow (B and E), appear to be targeting an area of the spinal cord that corresponds to their intended target area. Primary afferents cell bodies also appear stained in the DRG (C and F). Haematoxylin counterstain is seen in purple.

3.3.3 Prrxl1^{S119A} does not impact on the differentiation of glutamatergic spinal neurons

We attempted to use neuronal population markers to assess possible alterations in distribution or loss of such populations. Prrxl1 was previously reported to be expressed exclusively in glutamatergic neurons of the dorsal spinal cord (Rebelo et al., 2010). Moreover, the combinatorial expression of Prrxl1, Tlx3 and Lmx1b defined different glutamatergic sub-populations (Rebelo et al., 2010). Thus, we have focused our analysis on these markers. In Figure 22, α-Prrxl1 immunostaining presents no visible differences in terms of population distribution. The relative area occupied by Prrxl1^{+} neurons is comparable between the wild-type and Prrxl1^{S119A} spinal cord (Figure 22, white arrows). Prrxl1 expression in the DRG also seems to be similar between both genotypes. α-Tlx3

immunostaining, presented in Figure 23, also shows no detectable variations in terms of neuronal population distribution in the spinal cord and DRG. However, in Prrxl1^{S119A}, a discernible decrease in signal intensity is visible, which could suggest a reduction in Tlx3 expression in the dorsal spinal cord. Noteworthy, this decrease is not observed in the DRG (Figure 23C and F).

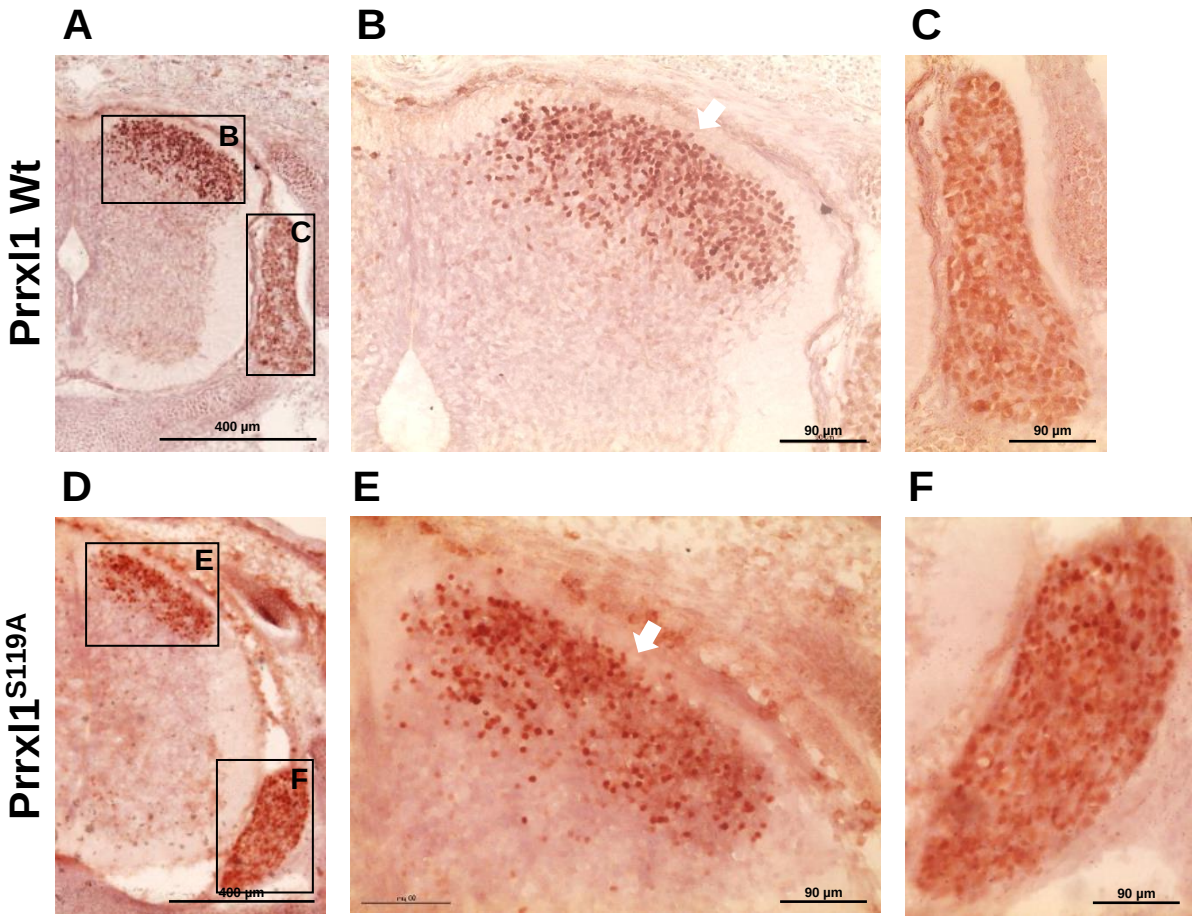

***Figure 22* - Anti-Prrxl1 immunostaining of wild-type and Prrxl1^{S119A} phospho-defective mutant E14.5 embryos.** General view of spinal cord (A, B, D and E), and dorsal root ganglia (C and F). Prrxl1 is expressed in the superficial dorsal horn of the spinal cord (white arrows, B and E), and in the DRGs (C and F). Localization of Prrxl1^{+} populations in Prrxl1^{S119A} appear to occur in the same regions as in the wild-type mice. Haematoxylin counterstain is seen in purple.

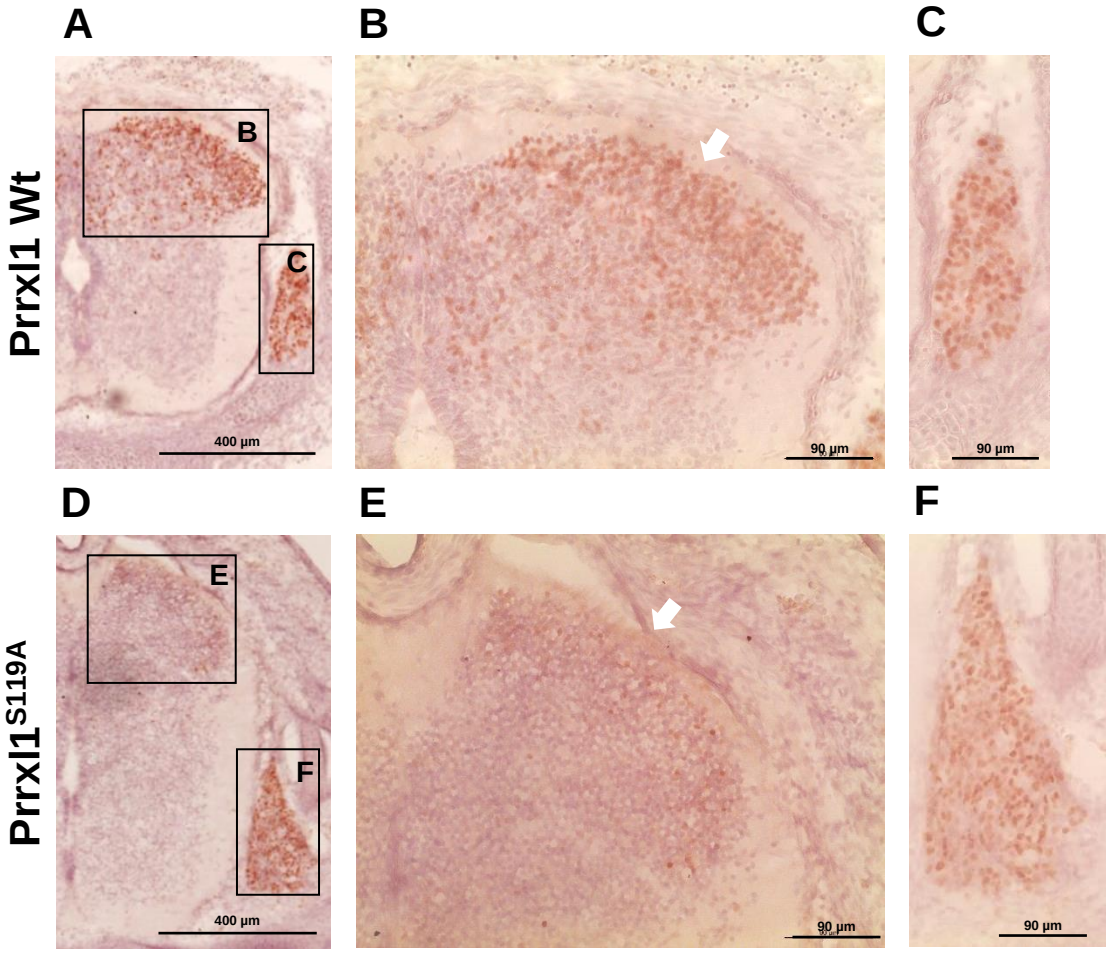

***Figure 23* - Anti-Tlx3 immunostaining of wild-type and Prrxl1^{S119A} mutant E14.5 embryos.** General view of spinal cord (A, B D and E), and dorsal root ganglia (C and F). Tlx3 is expressed in the dorsal horn of the spinal cord (white arrows, B and E), and in the DRGs (C and F). No major differences appear to be present in terms of population distribution when comparing Prrxl1^{S119A} mutants with Wild-type mice. However, a decrease in dorsal spinal cord signal intensity can be discerned in the Prrxl1^{S119A} phospho-defective mutant. This difference is not detectable in DRG. Haematoxylin counterstain is seen in purple.

3.4 Functional analysis

Since alterations in nociceptive sensitivity were detected in Prrxl1-null mice (Chen et al., 2001), and considering the importance of phosphorylation at S119 site for transcriptional activity shown in neuronal cell lines (Soares-Dos-Reis et al., 2017), we decided to better comprehend how Prrxl1^{S119A} phospho-mutation could impact on the sensitivity to noxious stimuli.

To assess this impact from a functional point of view, that is, how it translates to pain sensitivity in our Prrxl1^{S119A} knock-in mice, we performed a formalin injection protocol followed by western-blot analysis using an antibody against cFos protein. The formalin-

induced paw edema is commonly used as a chemical assay of injury-produced inflammatory pain. DRG neurons (L4-L5) projecting to the paw will sense the inflammation and will transmit the noxious stimuli to the ipsilateral side of the spinal cord, inducing a strong expression of cFos protein in spinal target neurons. Thus, the L4-L5 segment of the spinal cord of each tested animal was then extracted, and the dorsal aspect was divided into ipsi- and contralateral portions, which were analysed separately. This way, we were able to analyse possible variations related to the test (ipsilateral), while having an internal control at the same time (contralateral).

Our protocol consisted of injecting (sub-cutaneous plantar injection) 15 µL 5% formalin in saline (0,9% NaCl) on the right hind paw of each tested mouse (the left aspect of the dorsal spinal cord was the ipsilateral portion). It consisted in 12 mice, 6 wild-types and 6 harbouring the Prrxl1^{S119A} mutation. 3 of each genotype were used in a sham test (6 mice in total), in which only the vehicle (saline) was injected. The other group was injected with the 5% formalin solution. Only a few minutes after injection, mice injected with formalin solution had developed a swelling at the plantar region of the right hind paw (Figure 24).

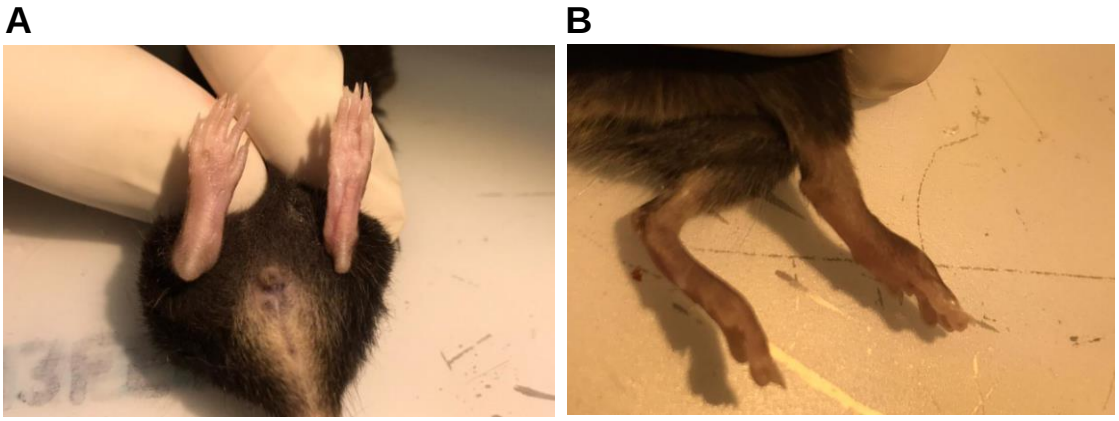

***Figure 24* – Formalin-induced paw edema** (indicated by the white arrow in both images). **A**: Plantar view; **B**: lateral view. A few minutes after injection, the right hind paw of mice injected with formalin solution swelled considerably, as a reaction to the chemical. The injected paw can clearly be differentiated by the presence of the swelling.

As previously mentioned, the selected portion of dorsal spinal cord was removed and separated in an ipsi/contralateral manner. SDS-PAGE of the protein extracts followed by western-blot against cFos and α-tubulin were performed. cFos was used as a marker for the activation of nociceptive neurons in the spinal cord (Gao & Ji, 2009; Hunt, Pini, & Evan, 1987), thus allowing us to visualize the degree of nociceptive stimulation in each of the conditions of the test (Figure 25, top half). For the same stimulus, an anesthetized animal would theoretically express lower amounts of cFos in the spinal cord, while a condition of

hyperalgesia would lead to a greater expression of that protein when compared to the control. Tubulin on the other hand was used as a loading control, to normalize our results across the various samples (Figure 25, bottom half).

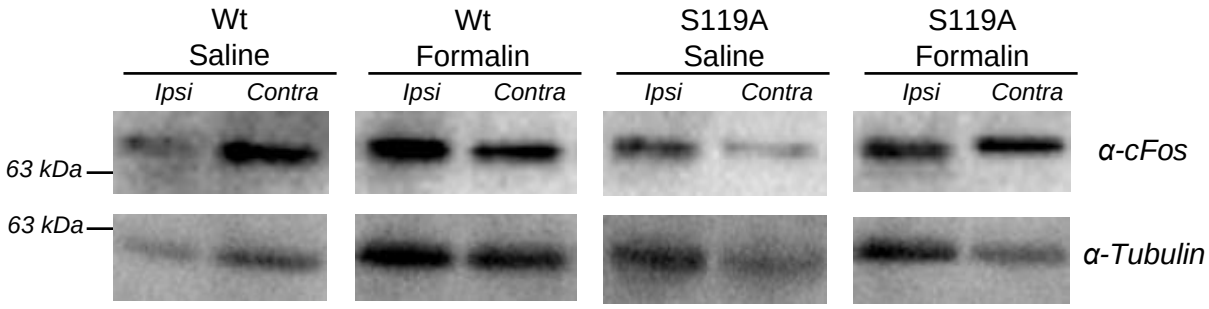

***Figure 25*– cFos quantification of formalin test**. cFos was used as a marker of stimulation of nociceptors in the spinal cord since its expression is induced by these stimuli. Tubulin was used as a loading control and for normalizing the obtained results.

These data were plotted and statistically analysed (Figure 26). No major variation was detected between genotypes of contralateral control samples, which is expected. Since nociceptive afferents from the right side of the body project to the left side of the dorsal spinal cord (ipsilateral side), the right (contralateral) side remains predominantly unaffected by cFos expression levels variation in response to the provoked noxious stimuli. Thus, no variation between conditions (injection type) should occur, nor variations between the two analysed genotypes should be detected.

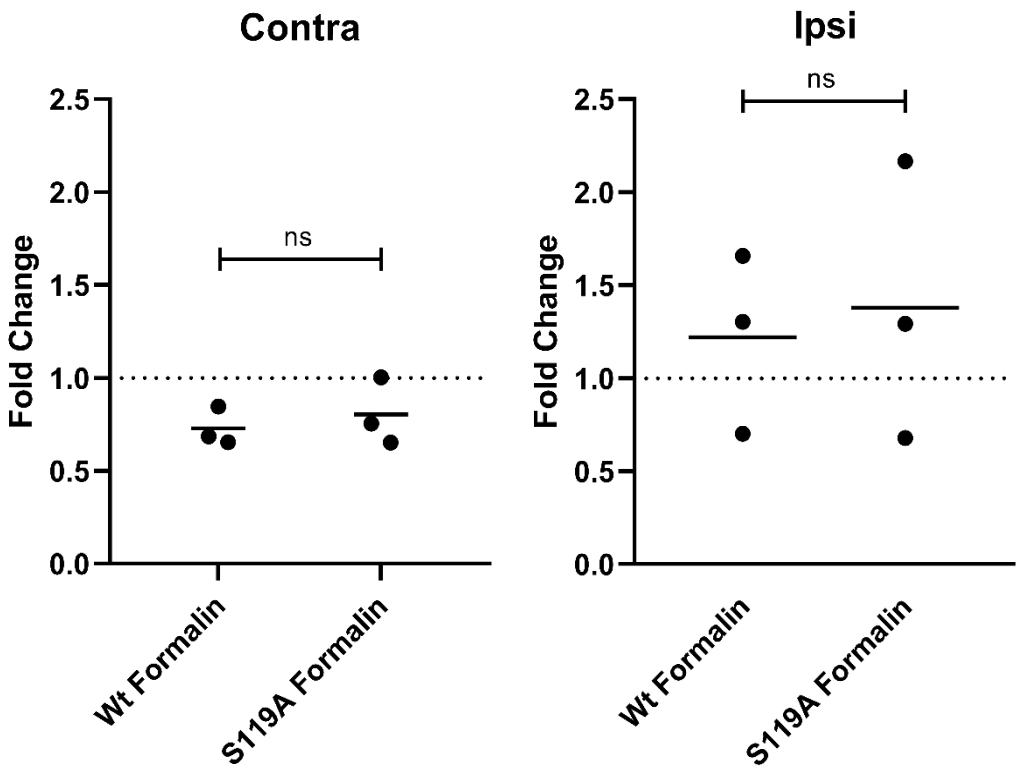

***Figure 26* - Formalin functional test analysis**. These graphics highlight cFos expression fold change across the various conditions of the test. The contralateral side (**A**) does not present statistically significant differences between wild-type and Prrxl1 S119A genotypes when injected with formalin, which was expected. Statistically, the S119A mutation does not appear to impact on the nociceptive sensitivity of the animal (ipsilateral side, **B**), since there are no significant variations between the two conditions. Results have been normalized to the corresponding sham test (example: Ipsi S119A w/Formalin normalized with Ipsi S119A w/Saline).

An increase in the expression of cFos is detected in both genotype when comparing the ipsilateral side to contralateral. This suggests that the formalin-induced hyperalgesia was successfully performed. However, a more detailed analysis shows a large dispersion within ipsilateral samples, suggesting that in some animals the cFos induction was not as robust as expected.

On the ipsilateral side, a slight increase in fold change comparatively to the wild-type mice can be observed in mice carrying the Prrxl1^{S119A} phospho-mutation. However, this increase is not significant from a statistical point of view.

CHAPTER 4

DISCUSSION

With this work, we aimed to characterize the impact of Prrxl1^{S119A} phospho-defective mutation in the development of the nociceptive system by using a knock-in mouse model. The mutant line was generated in the transgenic mouse facility at i3S. The first part of this work was the establishment of a genotyping method and the validation of the mutation. We were able to prove that the S119A mutation was successfully introduced and induced a specific electrophoretic mobility shift, similar to what was previously reported in *in* vitro studies (Soares-dos-Reis et al., 2014). The fact that we successfully reproduce a Prrxl1 dephosphorylation pattern associated to reduced Prrxl1 transcriptional activity in neuronal cells hinted toward the importance of this phospho-site in the establishment and/or maintenance of the nociceptive circuit. Our workflow was further guided by previous studies performed in Prrxl1-null mutant mice, which described time-specific abnormalities caused by Prrxl1 deletion (Chen et al., 2001; Rebelo et al., 2006; Rebelo et al., 2010). Among these defects were nociceptive afferents innervation delays, morphological abnormalities due to cell death of Prrxl1-dependent neurons, and reduced sensitivity to noxious stimuli.

We aimed to better comprehend how Prrxl1^{S119A} phospho-defective mutation impact on gene regulation of Prrxl1 target genes. Prrxl1 is an important transcription factor, especially during the development of the nociceptive system, mainly at the embryonic stages (Chen et al., 2001). Although we still don't know If cell death occurs in Prrxl1^{S119A} mutant spinal cord as it was observed in Prrxl1-null mutant mice from E17.5 onward (Chen et al., 2001), we studied Prrxl1 targets gene expression during embryonic development, at two distinct timepoints, E13.5 and E14.5, to avoid any effects related to neuronal loss. The selection of Prrxl1 targets for qPCR analysis was made using a comprehensive list of putative Prrxl1 target genes generated from the integration of binding events (ChIP-seq) with microarray expression data in DRG and dorsal SC of E14.5 Prrxl1-null embryos (Monteiro, unpublished). From these data, candidates were chosen according to their fold changes, prioritizing those with higher variations. Firstly, we conducted pilot tests using E13.5 embryos using dSC and DRG. E13.5 qPCR analysis produced results which could indicate some degree of Prrxl1 target alterations, namely a tendency for CCK and CCDC68 overexpression in DRG and a decrease in GalrI and Tlx3 expression in the dorsal SC. Neurogenesis, however, is still underway during this embryonic day. We decided to repeat the analysis using the most promising candidates using E14.5 tissues, a developmental age when neurogenesis is already complete. Only Prrxl1 target CCDC68 appeared to be deregulated (under-expressed) in a statistically significant manner. Through the obtained data, one might be led to think that the phospho-defective mutation being studied does not impact on Prrxl1 targets expression in a major way. However, and while that may be possible, another circumstance might be the cause of such results. Various cell populations

are present in the spinal cord. Each neuronal type is characterized by specific combinatorial expression of determined sets of transcription factors (Lai et al., 2016). As such, Prrxl1 is not expressed broadly through the dorsal spinal cord, but rather in a couple of superficial laminae (I to III) of the dorsal horn. When dissecting embryonic spinal cords, the procedure attempts to separate its dorsal side from its ventral side, in order to enrich Prrxl1^{+} neurons and thereby increase the possibility to detect gene variations in such populations. However, even when dissecting the dorsal part of the spinal cord (which in itself might not always result in a similar population-wise separation), several populations in which Prrxl1 is not expressed are present in the retrieved spinal cord section used for RNA extraction. These Prrxl1 negative populations might interfere with qPCR detection since some of Prrxl1 target genes may also be present in those cells. This in turn may lead to a "drowning out" effect of potentially deregulated Prrxl1 targets expression in Prrxl1^{+} populations.

Furthermore, it is important to consider that phosphorylation mechanisms allow to fine tune or switch the activity of a given protein in different cell types. Considering that Prrxl1 is expressed in several glutamatergic neuronal populations (Rebelo et al., 2010), one may hypothesize that the phosphorylation at Prrxl1 S119 site may be required for the regulatory mechanisms in a specific cell population, but not overall. This means that even though the lack of phosphorylation at Prrxl1^{S119A} phospho-site may strongly impact on a determined Prrxl1^{+} population (thus affecting Prrxl1 targets expression in that particular cell type), other populations might not be affected. In turn, this can lead to just a slight variation of Prrxl1 targets expression as a whole, diluting any possibly clearer deregulations at Prrxl1^{+} populations that are also Prrxl1 p119-dependent. Therefore, these slight variations may not be detectable through the methods we used, which means that we may perceive that no variations are occurring, when in fact they are present. Ways to tackle this issue involve the use of more refined methods to study individual populations, or, at least, being able to study more selected and better defined groups of populations, where the dilution effect would not be present or at least be present in a substantially lower degree. Nonetheless, further analysis to Prrxl1 target gene expression in this model are necessary. Also, tackling the statistical significance problems through the increase of number of tested samples (*n*) would be important and should be performed in the future.

Worthwhile considering is the somewhat constant variation among samples. This variation is, at this time, one of the biggest challenges this work has been presenting us, since most experiments end up leading to more or less inconclusive results, from which we can only infer deregulation tendencies in certain genes. Even though we do not know exactly what is causing the observed variations, a possible explanation dwells in the fact that various

populations are being studied at once. This inherent variability of neuronal types could not only be causing the dilution effect previously approach, which can in itself prevent or difficult this study, but also the variability amongst individuals that causes considerable deviations between samples. As previously discussed, more refined and specific methods that would allow us to study populations separately or in small groups could in theory prove valuable to tackle this problematic, but also the one regarding the dilution effect.

We also looked at putative defects in the dSC morphology of our Prrxl1^{S119A} mutants. The histological studies performed in our knock-in mouse model did not indicate the presence of any major abnormalities, both in terms of fibre innervation and distribution of glutamatergic neurons. We conducted these tests mostly during embryonic stages (E14.5). We found no trace of delayed fibre innervation at this timepoint. In Prrxl1-null mice, nociceptive afferents entrance and ingrowth in the spinal cord suffers a delay: while in wild-types the fibres reach and penetrate the dorsal root entry zone (DREZ) of the spinal cord at around E13.5, in Prrxl1$^{-/-}$ mice this event only occurs later on. This difference in afferent projection timings was not found in our phospho-defective mutant, since both wild-type and Prrxl1^{S119A} mice displayed similar results.

Population-wise, Prrxl1^{+} neuronal populations and Prrxl1 expression appeared unaffected by the presence of Prrxl1^{S119A} phospho-defective mutation. Although Prrxl1 negatively regulates its own promoter (C. B. Monteiro et al., 2014), the phosphorylation at s119 has no impact on this regulation mechanism. This observation is in line with what was observed in neuronal cell lines, in which overexpression of Prrxl1^{S119A} variant did not alter the transcriptional activity of this protein on the Prrxl1 promoter (Soares-dos-Reis et al., 2014) (see Figure 10 in introduction section). Unlike Prrxl1, immunohistochemical (IHC) analysis showed that Tlx3^{+} populations were clearly less reactive in the Prrxl1^{S119A} spinal cord. Tlx3^{+} neurons in the DRGs displayed a signal intensity comparable to that of wild-types. This suggests a specific reduction of Tlx3 expression in the dorsal SC, but not in the DRG, pointing out to a tissue/cell-specific role for S119 phospho-site. Despite the changes in Tlx3 expression in phospho-mutant mice, Tlx3^{+} populations appeared normal in terms of laminal position and cell number, with no alterations to report when compared to the wild-type.

Worth mentioning that the reduced expression of Tlx3^{+} in Prrxl1^{S119A} spinal cords verified in the IHC analysis, is further supported by our qPCR data. Indeed, qPCR analysis in dorsal SC of E13.5 embryos showed a decrease in Tlx3 expression in Prrxl1^{S119A} although, as formerly referred, these results are just a trend and were not statistically significant, possibly due to a combination of factors ranging from sample size to sample variability. However,

when considering the IHC data, Tlx3 deregulation appears to be present and should be further assessed, both using a higher number of samples, but also on other embryonic ages.

Furthermore, we used a functional test to assess pain sensitivity in adult mice through formalin injection, followed by western blot analysis of cFos, a marker of nociceptive neurons activation. We used vehicle-only injections to normalize both the ipsi- and the contralateral sides of the medulla, which allowed us to interpret and visualize the dada. The results revealed a slight overexpression on the side corresponding to the injected hind paw (ipsilateral). Despite the apparent trend of increased response to noxious stimuli, the data were statistically insignificant due to the huge variation within groups.

Some issues, however, arise regarding the experiment itself, and are worth approaching. A simple, yet necessary, way to improve this test is increasing the *n*. By increasing the number of samples, we could in theory receive a clearer answer regarding the true nature of Prrxl1^{S119A} mice nociceptive sensitivity. By utilizing such a low *n*, we risk being misled by possible outlying data (that may easily be caused by variations in the local and amount of formalin injected) that might exist in our samples, while increasing it reveals the true tendency of each of the genotypes when responding to a noxious stimulus. Another important matter to discuss is the presence of variation in the ipsilateral side that is not matched by a variation on the contralateral side. The contralateral side remains relatively unscathed during the test, since cFos expression increase occurs in the ipsilateral side. A possible explanation to this variation could be a slight delay during the experiment. cFos (over)expression after noxious stimulation is transient, with the protein peaking at around 90 minutes (Gao & Ji, 2009). When the peak is overcome, cFos protein starts decreasing until it reaches basal levels, which only occurs anywhere from 8 to 24 hours (Gao & Ji, 2009). In the case of some of the tested animals, the waiting period between injection and sacrifice (and subsequent dissection) might have surpassed this peak, which may have contributed to an overall lowering of cFos protein in the spinal cord, thus allowing for the variability that can be observed on the ipsilateral side but not on the contralateral side.

Moreover, we intend to upscale and improve this test in the future, by increasing the total number of analysed samples and enhancing the timing for dissection to avoid the issues caused by overcoming the cFos pea. Additionally, while the present work obtained the functional test results through western blot band quantification, we intend to assess possible alterations through IHC analysis of cFos^{+} neurons after noxious stimulation. This technic allows for a cell-specific analysis, providing a visual representation of which neuronal populations respond to a predetermined noxious stimulus, whilst solving the previously

discussed dilution issues. Quantification itself can be attained by counting the number of activated neurons per dSC hemi-section.

Because phosphorylation allows for precise control of the activity of a given protein in different cell contexts, it is expected that phosphorylation at Prrxl1^{S119A} will affect specific neuronal populations, which are involved in the processing of different pain modalities. Therefore, the formalin-induced inflammatory pain test should also be complemented with others, targeting other types of noxious stimuli, such as temperature (e.g. hot- and cold-plate tests) or pressure (using, for example, Von Frey filaments) tests. This would allow us to study different afferents/populations on a functional level other than those responsible for chemical nociception (the type of stimulus formalin injection would trigger).

Broadly speaking, our work tried to follow previous reported data regarding the Prrxl1-null mouse model. In it, various abnormalities were detected, ranging from fibre innervation delays and neuronal death in the spinal cord, to desensitisation toward noxious stimuli and decreased lifespan. However, these studies possessed a “time dimension” our study did not, at least not as extensively, have. Various defects reported in Prrxl1$^{-/-}$ were observed at different developmental ages. This means that, since our study mostly focused on E13.5 and E14.5 embryos, it would be ideal to study possible fibre innervation defects previously observed around those ages in Prrxl1$^{-/-}$ mice (Chen et al., 2001). However, when considering neuronal loss in the dorsal SC, this age might not be the most appropriate, since in the constitutive knock-out, ablation of Prrxl1-dependent neurons only began around embryonic day 17.5 (Chen et al., 2001).

In addition, and also considering the age factor, studies similar to this one, but considering a phospho-mimetic mutant for the S119 phospho-site (Prrxl1^{S119D}), could also prove valuable, especially when considering the time-specific variation of Prrxl1 phosphorylation profile. The substitution of S119 for an aspartate would cause a permanent state of emulated phosphorylation at the 119-site, the opposite of Prrxl1^{S119A} mouse model, which avoids phosphorylation at that same site. Likewise, S119D, like S119A, was reported to affect Prrxl1 transcriptional activity by *in vitro* studies (Soares-Dos-Reis et al., 2017), which by itself would make for an interesting study case (see Figure 10 in introduction section). Particularly, studying this phospho-mutation in more advanced ages, such as postnatally, could prove useful since as development progresses, a gradual dephosphorylation of Prrxl1 occurs (Soares-dos-Reis et al., 2014). This Prrxl1^{S119D} mouse model would make it possible to study what effects may occur if the Prrxl1 119 site remains phosphorylated through-out development and into postnatal ages, where a dephosphorylated version of Prrxl1 would

otherwise be present. The combination of both characterizations could help assess the importance of the S119 site in the regulation of Prrxl1 through-out development.

In conclusion, we successfully validated the Prrxl1^{S119A} mouse model as we verified that this mutation caused an overall dephosphorylation of the protein (through the impairment of phosphorylation at the S119 site), similar to the one observed *in vitro* in previous studies (Soares-dos-Reis et al., 2014). However, we were not able to discern major if any alterations in our *knock-in* mouse model such as phenotypical defects in the pain pathway, changes in protein expression related to the phospho-defective mutation or spinal cord morphology variations. Most of our results turned to be inconclusive due mainly to sample variability and further studies are required to fully characterize the Prrxl1^{S119A} phospho-defective mutation. Despite this lack of definitive results, this work generated some pilot data that will help us in the future in the design of strategies aimed at better characterizing the impact of S119 phosphorylation in the development of nociceptive neurons. Widening the spectrum of analysed ages, as well as using more refined technics that allow for the study of independent, or small groups of, populations, and increasing the amount of samples are all valid ideas that will be put into practice in the near future.

REFERENCES

Basbaum A. I., & Jessell T. M. (2000). The perception of pain. In Kandel, E. R., Schwartz J. H., & Jessell T. M. (Eds.), *Principles of Neural Science* (pp. 472-479). New York: McGraw-Hill.

Breivik, H., Collett, B., Ventafridda, V., Cohen, R., & Gallacher, D. (2006). Survey of chronic pain in Europe: prevalence, impact on daily life, and treatment. *European Journal of Pain, 10*(4), 287-333. doi:10.1016/j.ejpain.2005.06.009

Caspary, T., & Anderson, K. V. (2003). Patterning cell types in the dorsal spinal cord: what the mouse mutants say. *Nature Reviews Neuroscience 4*(4), 289-297. doi:10.1038/nrn1073

Chen, Z. F., S., R., F., W., A.B., M., H., B., D., L., . . . Anderson, D. J. (2001). The Paired Homeodomain Protein DRG11 Is Required for the Projection of Cutaneous Sensory Afferent Fibers to the Dorsal Spinal Cord. *Neuron, 31*, 59-73.

Cheng, L., Arata, A., Mizuguchi, R., Qian, Y., Karunaratne, A., Gray, P. A., . . . Ma, Q. (2004). Tlx3 and Tlx1 are post-mitotic selector genes determining glutamatergic over GABAergic cell fates. *Nature Neuroscience, 7*(5), 510-517. doi:10.1038/nn1221

Cheng, L., Samad, O. A., Xu, Y., Mizuguchi, R., Luo, P., Shirasawa, S., . . . Ma, Q. (2005). Lbx1 and Tlx3 are opposing switches in determining GABAergic versus glutamatergic transmitter phenotypes. *Nature Neuroscience, 8*(11), 1510-1515. doi:10.1038/nn1569

Cohen, P. (2000). The regulation of protein function by multisite phosphorylation - a 25 year update. *Trends in Biochemical Sciences*, 596-601.

Crofford, L. J. (2015). Chronic pain: where the body meets the brain. *Transactions of the American Clinical and Climatological Association, 126*.

Dubuisson, D., & Dennis, S. G. (1977). The formalin test: a quantitative study of the analgesic. *Pain, 4*, 161-174.

Farley, A., Johnstone, C., Hendry, C., & McLafferty, E. (2014). Nervous system: part 1. *Nursing Standard*.

Gao, Y.-J., & Ji, R.-R. (2009). c-Fos or pERK, Which is a Better Marker for Neuronal Activation and Central Sensitization After Noxious Stimulation and Tissue Injury? *The Open Pain Journal, 2*, 11-17.

Gong, N., Huang, Q., Chen, Y., Xu, M., Ma, S., & Wang, Y.-X. (2014). Pain Assessment Using the Rat and Mouse Formalin Tests. *Bio-Protocol, 4*(21). doi:10.21769/BioProtoc.1288

Helms, A. W., & Johnson, J. E. (2003). Specification of dorsal spinal cord interneurons. *Current Opinion in Neurobiology, 13*(1), 42-49. doi:10.1016/s0959-4388(03)00010-2

Hunskaar, S., Fasmer, O. B., & Hole, K. (1985). Formalin test in mice, a useful technique for evaluating mild analgesics. *Journal of Neuroscience Methods, 14*, 69-76.

Hunt, S. P., Pini, A., & Evan, G. (1987). Induction of c-fos-like protein in spinal cord neurons following sensory stimulation. *Nature, 328*, 632-634.

Hunter, T. (2012). Why nature chose phosphate to modify proteins. *Philosophical Transactions of the Royal Society of London Biological Sciences, 367*(1602), 2513-2516. doi:10.1098/rstb.2012.0013

Jensen, T. S., & Finnerup, N. B. (2014). Allodynia and hyperalgesia in neuropathic pain: clinical manifestations and mechanisms. *The Lancet Neurology, 13*(9), 924-935. doi:10.1016/s1474-4422(14)70102-4

Julius, D., & Basbaum, A. I. (2001). Molecular mechanisms of nociception. *Nature*. 413(6852), 203-210.

Lai, H. C., Seal, R. P., & Johnson, J. E. (2016). Making sense out of spinal cord somatosensory development. *Development, 143*(19), 3434-3448. doi:10.1242/dev.139592

Loeser, J. D., & Treede, R. D. (2008). The Kyoto protocol of IASP Basic Pain Terminology. *Pain, 137*(3), 473-477. doi:10.1016/j.pain.2008.04.025

Merskey, H., Mumford, J. M., Nathan, P. W., Noordenbos, W., & Sunderland, S. (1994). Pain terms: a current list with definitions and notes on usage. *International Association for the Study of Pain*.

Monteiro, C., Rebelo, S., Galhardo, V., Reguenga, C., & Lima, D. (2011). Postnatal expression of the homeobox gene Prrxl1 (Drg11) is increased in inflammatory but not neuropathic pain. *European Journal of Pain, 15*(5), 477-481. doi:10.1016/j.ejpain.2010.10.007

Monteiro, C. B., Costa, M. F., Reguenga, C., Lima, D., Castro, D. S., & Monteiro, F. A. (2014). Paired related homeobox protein-like 1 (Prrxl1) controls its own expression by a transcriptional autorepression mechanism. *FEBS Letters, 588*(18), 3475-3482. doi:10.1016/j.febslet.2014.08.006

Muller, T., Pierani, A., Lewin, G. R., Brohmann, H., Heppenstall, P. A., Jessell, T. M., & Birchmeier, C. (2002). The Homeodomain Factor Lbx1 Distinguishes Two Major

Programs of Neuronal Differentiation in the Dorsal Spinal Cord. *Neuron, 34*, 551-562.

Murray, C. W., Porreca, F., & Cowan, A. (1988). Methodological refinements to the mouse paw formalin test. *Journal of Pharmacological Methods, 20*, 175-186.

Nahin, R. L. (2015). Estimates of pain prevalence and severity in adults: United States, 2012. *Journal of Pain, 16*(8), 769-780. doi:10.1016/j.jpain.2015.05.002

Purves, D., Augustine, G. J., Fitzpatrick, D., Hall, W. C., LaMantia, A. S., McNamara, J. O., & Williams, S. M. (2004). *Neuroscience*. Sinauer Associates, Inc.

Raja, S. N., Carr, D. B., Cohen, M., Finnerup, N. B., Flor, H., Gibson, S., . . . Vader, K. (2020). The revised International Association for the Study of Pain definition of pain: concepts, challenges, and compromises. *Pain*. doi:10.1097/j.pain.0000000000001939

Rebelo, S., Chen, Z. F., Anderson, D. J., & Lima, D. (2006). Involvement of DRG11 in the development of the primary afferent nociceptive system. *Molecular and Cellular Neuroscience, 33*(3), 236-246. doi:10.1016/j.mcn.2006.07.013

Rebelo, S., Reguenga, C., Lopes, C., & Lima, D. (2010). Prrxl1 is required for the generation of a subset of nociceptive glutamatergic superficial spinal dorsal horn neurons. *Developmental Dynamics, 239*(6), 1684-1694. doi:10.1002/dvdy.22305

Regadas, I., Soares-Dos-Reis, R., Falcao, M., Matos, M. R., Monteiro, F. A., Lima, D., & Reguenga, C. (2014). Dual role of Tlx3 as modulator of Prrxl1 transcription and phosphorylation. *Biochimica et Biophysica Acta, 1839*(11), 1121-1131. doi:10.1016/j.bbagrm.2014.08.007

Rexed, B. (1954). A cytoarchitectonic atlas of the spinal coed in the cat. *Journal of Comparative Neurology*, 100(2), 297-379.

Soares-Dos-Reis, R., Pessoa, A. S., Dias, A. F., Falcao, M., Matos, M. R., Vitorino, R., . . . Reguenga, C. (2017). A role for prolyl isomerase PIN1 in the phosphorylation-dependent modulation of PRRXL1 function. *Biochemical Journal, 474*(5), 683-697. doi:10.1042/BCJ20160560

Soares-dos-Reis, R., Pessoa, A. S., Matos, M. R., Falcao, M., Mendes, V. M., Manadas, B., . . . Reguenga, C. (2014). Ser119 phosphorylation modulates the activity and conformation of PRRXL1, a homeodomain transcription factor. *Biochemical Journal, 459*(3), 441-453. doi:10.1042/BJ20131014

Todd, A. J. (2010). Neuronal circuitry for pain processing in the dorsal horn. *Nature Reviews Neuroscience, 11*(12), 823-836. doi:10.1038/nrn2947

Treede, R. D. (2018). The International Association for the Study of Pain definition of pain: as valid in 2018 as in 1979, but in need of regularly updated footnotes. *Pain Reports, 3*(2), e643. doi:10.1097/PR9.0000000000000643

Yam, M. F., Loh, Y. C., Tan, C. S., Khadijah Adam, S., Abdul Manan, N., & Basir, R. (2018). General Pathways of Pain Sensation and the Major Neurotransmitters Involved in Pain Regulation. *International Journal of Molecular Sciences, 19*(8). doi:10.3390/ijms19082164